Cartilage-inspired, lipid-based boundary-lubricated hydrogels

Cartilage-inspired, lipid-based boundary-lubricated hydrogels

Weifeng Lin[1], Monika Kluzek[1], Noa Iuster[1], Eyal Shimoni[2], Nir Kampf[1], Ronit Goldberg*[1,3] and Jacob Klein*[1]

[1] Dept. of Materials and Interfaces, Weizmann Institute of Science, Rehovot 76100, Israel
[2] Dept of Chemical Research Support, Weizmann Institute of Science, Rehovot 76100, Israel
[3] Present address: Liposphere Ltd., Pinhas Sapir Street 3, Nes Ziona 7403626, Israel

*Corresponding author. Email: ronit.goldberg@lipo-sphere.com; Jacob.klein@weizmann.ac.il

Abstract

The lubrication of hydrogels arises from fluid or solvated surface-phases. In contrast, the lubricity of articular cartilage has been at least partially attributed to non-fluid, lipid-exposing boundary layers. We emulate this in synthetic hydrogels by incorporating trace lipid concentrations to create a continuously-renewing, molecularly-thin, lipid-based boundary layer. We observe a reduction in friction and wear by up to a 100-fold or more relative to the lipid-free gel, over a wide range of conditions. This persists when gels are dried and then re-hydrated. Our approach may provide a method for sustained, extreme lubrication of hydrogels in areas from tissue engineering to clinical diagnostics.

Synthetic hydrogels are widely used in biomedical and other applications (*1-3*), and their lubricity is crucial for their efficient function whenever surfaces slide past each other. The lubrication is attributed to fluid interfacial layers intrinsic to the gels, such as exuded liquid films or solvated flexible polymers at their surfaces (*4-7*). In contrast, biological materials like articular cartilage remain well lubricated over a lifetime of sliding and wear. The low friction of cartilage has been attributed to fluid pressurization as supporting much of the load (an effect which does not apply in synthetic hydrogels (*8*)), while its boundary lubrication has been attributed to non-fluid boundary layers at its surface (*9-12*). These layers expose phosphatidylcholine (PC) lipids whose highly-hydrated phosphocholine head-groups may reduce friction via the hydration lubrication mechanism (*13, 14*). The maintenance of such boundary layers following frictional wear occurs through cellular replenishment and self-assembly of their components (*13, 15, 16*), including hyaluronan, lubricin and especially PC lipids (*17-21*), which reduce friction at the slip plane via their hydrated phosphocholine head-groups (*11*). These components are ubiquitous both in cartilage and in the surrounding synovial fluid (*15, 19, 20*), and thus readily available to maintain the lubricating layer at the articular surface.

We adapt this mechanism to lubricate synthetic hydrogels via the incorporation of small amounts of PC lipids to form micro-reservoirs throughout the gel bulk, by mixing a low concentration of PC lipids with the desired monomer solution, then polymerizing and cross-linking to form the hydrogel. The reduction in friction and wear is attributed to a lipid-based boundary layer at the hydrogel surface, which is continually reconstructed as it wears, through progressive release of lipids, as indicated schematically in fig. 1. We have used this approach to create several different self-lubricating hydrogels, of both biological and synthetic

polymers (Supplementary Discussion, *SD 1*); here we focus on the widely exploited (*1*) poly(hydroxyethylmethacrylate), pHEMA, hydrogel.

[FIGURE 1 HERE]

Hydrogels were prepared either lipid-free, or with low concentrations of the PC lipids dimyristoylphosphatidylcholine (DMPC) or hydrogenated soy phosphatidylcholine (HSPC) added in the form of multilamellar vesicles, MLVs (though smaller unilamellar vesicles may also be present, Methods section 2). These lipids were chosen as they are respectively above and below their gel-to-liquid transition – known to affect lubrication (*22*) - at room and physiological temperatures. Their distribution is revealed by freeze-fracture cryo-scanning electron microscopy (cryo-SEM) and confocal fluorescence microscopy (Methods section 6), as seen in figure 2 (see also *SD 4*). The lipid-free hydrogel, fig. 2A, shows

[FIGURE 2 HERE]

a featureless internal surface, as expected at this resolution. Figs. 2B-F show the incorporated DMPC and HSPC MLVs within the hydrogel bulk. These are sequestered in clusters either as spherical micro-reservoirs filled with roughly spherical vesicles (DMPC, figs. 2B-D), whose size is consistent with dynamic-light-scattering measurements on the liposome dispersions (Methods section 2), or in less regular clusters (HSPC, fig. 2E, F). Rheometrically-determined mechanical properties (Methods section 4), fig. 2G, reveal that the hydrogel storage modulus G' (>> G'', the loss modulus) varies over the frequency range 0.1–10 Hz by ca. 30% or less between lipid-free and PC-incorporating hydrogels.

Sliding friction F_s between the hydrogel and a polished stainless-steel surface, as well as surfaces of other materials (*SD 7*), was examined over a range of loads F_n, corresponding to different mean contact stresses P, and sliding velocities v_s (Methods section 7 and *SD 12*),

yielding the coefficient of sliding friction $\mu = F_s/F_n$. Fig. 3A shows the tribometer configuration, with representative directly-recorded traces from which F_s and thus μ is determined, while figs. 3B, C reveal and quantify the transfer of lipids between gel and steel surface during contact and sliding.

[FIGURE 3 HERE]

Figs. 3D and 3E show the variation of μ with load for the two lipids used, at room (25 ℃) and at physiological temperature (37 ℃). A reduction in friction is seen for the lipid-incorporating relative to the lipid-free gels. For the former, μ is in the range ca. 0.02 at lower loads to 0.005 at the higher loads; for the lipid-free gel, at low loads and contact stresses, $0.5 \lesssim \mu \lesssim 1$ was measured (similar to earlier measurements of high friction for steel sliding against pHEMA hydrogels (*23*)), while for P higher than ca. 0.5 MPa the metal surface would deform or tear the gel, without sliding (fig. 3A, see Methods section 7). The reduction in friction (figs. 3D, E) arising from the lipid-incorporation thus ranges from ca. 25-fold to 100-fold or more at the higher loads and contact pressures. While both lipids reduce the friction relative to the lipid-free gel, at room temperature the DMPC is slightly more lubricious at low loads, while at 37 ^{o}C the HSPC lipids reduce friction more. We attribute this to the interplay between head-group hydration and bilayer robustness for the two lipids, arising from their different phase states (*22*). Fig. 3F shows the near-constant value of μ with sliding velocity over some 3 orders of magnitude in v_s, a clear signature of boundary as opposed to fluid-film lubrication.

Incorporating lipids within the bulk hydrogel resulted in far-lower friction than when the gels were exposed to lipids externally, as shown in fig. 4A. For lipid-incorporating hydrogels sliding under water $\mu \approx 0.01$, compared with $\mu \approx 0.06$–0.08 for lipid-free gels sliding immersed a PC-MLV dispersion; while for lipid-free hydrogels incubated

[FIGURE 4 HERE]

overnight in PC-MLV dispersions, then measured in water, $\mu \approx 0.08–0.15$. In the latter case the friction rises sharply with sliding time (*SD 2*). Lubrication by such external application of lipids is thus far less effective than when they are bulk-incorporated. For the case of sliding in a liposome dispersion, this is attributed to their poor access into the inter-surface region which arises from the very large distortion energy required for liposomes to enter the inter-surface gap (*SD 8*). For the case of sliding following overnight lipid adsorption, the lubrication deteriorates rapidly through wear once the external PC source is removed (*SD 2*).

On fully drying the lipid-incorporating gels, followed by their rehydration (Methods section 9), the friction returns to its low value, and the lubrication is once again self-sustaining (figure 4B). This robustness to drying/rehydration has implications in particular for coating by, and storage of hydrogels. Finally, not only the friction but also wear and surface damage were reduced by the incorporated lipids. Fig. 4C compares wear of the lipid-free hydrogel with that of a DMPC-MLV-incorporating hydrogel following 2 hours of sliding. In these conditions the wear of the lipid-free pHEMA gel surface was 57±3 μm for a 1 N load, while wear of the lipid-incorporating gel (where $\mu \approx 0.01$ throughout the 2 hours of sliding) was below the detection limit (± 3 μm) of the tribometer even for a tenfold-larger load. This implies that such gels could resist significant wear over large numbers of sliding cycles (*SD 13*). The effect of low surface-wear/damage manifests at a higher load as shown in fig. 4D. The lipid-free gel is damaged and torn following just a few seconds of back-and-forth motion of the steel countersurface. This is attributed to the high friction strongly shearing the gel, and arises because the shear stress σ_s at the gel surface, given by $\sigma_s = \mu P \approx 10^6$ N/m^2, where the friction coefficient $\mu \approx (0.5–1)$ and the mean pressure $P \approx 1.5$ MPa, greatly exceeds the gel shear modulus $G' \approx 6 \times 10^4$ /m^2. At the same time the lipid-incorporating hydrogel (fig. 4D left, for which $\mu \approx 0.01$, and $\sigma_s = \mu P \approx 10^4$ N/m^2 is much less than G') is barely affected after a full hour

of sliding under this load. We note that following the 1 hr sliding at this high load and contact stress (1.53 MPa), the surface of the liposome-containing gel has worn by 9±3 μm (Methods, section 7, and *SD 11*); yet despite this removal-by-wear of the original gel surface, the frictional force remains unchanged with $\mu \approx 0.01$ throughout. Since this extent of surface wear far exceeds the thickness of any boundary lubricating layer or size of the micro-reservoirs (fig. 2), it is clear that such layers are continuously renewing as friction abrades the surface, as indicated in fig. 1. Hydrogels conform affinely when compressed by a counter-surface already at quite low contact stresses (higher than a fraction of an atm, see *SD 14*). Thus one expects the lubricating lipids to spread over the entire hydrogel contact area, as long as the sliding amplitude exceeds the mean inter-micro-reservoir spacing of a few μm.

Sliding takes place through hydration-lubricated slip between the exposed hydrated headgroups of the lipid bilayers or liposomes (*SD 6*). These are extracted by interfacial shear - due to the sliding - from the surface-exposed micro-reservoirs (figs. 1 and 2) and are thereby spread to coat the opposing (gel and metal) surfaces (*SD 5*). The zwitterionic phosphocholine headgroups adhere both to the negatively charged (*24*) pHEMA surface, which is rich in dipolar hydroxyl groups (*25*) (such dipole-charge interactions may also help to localize the vesicles within the micro-reservoirs), and to the negatively-charged stainless-steel counter-surface (*26*), as seen by atomic force microscopy imaging (*SD 3,4*). More directly, we see transfer of fluorescently labelled gel-incorporated lipids to the sliding steel sphere countersurface. The area covered by the transferred lipids can be imaged, as in fig. 3B, and its thickness evaluated from their total calibrated fluorescence intensity (fig. 3C and Methods, section 11). This shows that the lipid layer on the metal surface is 1.5±0.5 bilayers thick, consistent with hydration lubrication at the slip plane between metal-attached and gel-attached bilayers as indicated in fig. 1. Similar hydration lubrication by PC boundary layers on model substrates (*13, 27*) yields even

lower friction, $\mu \approx 0.001$ or less, than observed with our hydrogels (where $\mu \approx 0.005$–0.02). This reflects the softer and rougher nature of our substrates, with consequent additional pathways for frictional dissipation, such as viscoelastic losses, relative to these earlier studies where rigid and extremely smooth substrates were used (*22, 27, 28*). Evidence for this is provided by the variation of μ for pHEMA gels of different moduli, induced by varying the cross-linker density within the lipid-incorporating gels, where softer gels show higher sliding friction (*SD 9*).

The self-renewal of the lubricating boundary layer, as the hydrogel abrades under friction, is attributed to its continuous healing through availability of lipids at the surface, as micro-reservoirs of the PC vesicles within the gel become progressively exposed and sheared by the countersurface, fig. 1. A more detailed consideration (Methods section 10) shows that the total volume of lipids available at the gel surface from reservoirs transected by it would be sufficient to form a lipid film of thickness d given by

$$d \approx 2\phi R_0 \qquad (1)$$

where ϕ is the mean volume fraction of lipids incorporated in the bulk hydrogel, and R_0 is the radius of a micro-reservoir. R_0 could be varied by changing the concentration of lipids incorporated within the gel (*SD 10*). Taking, as in the present experiments, $R_0 \approx 1.5$ μm (figs. 2 B, C) and $\phi = 0.012$ (Methods section 2) gives d ≈ 36 nm, which is equivalent to the thickness of some 7–8 bilayers of DMPC. This is more than sufficient for hydration lubrication between a bilayer or even a compressed vesicle layer attached on each of the opposing surfaces (*22, 28*), indicating that the mechanism shown in fig. 1 can amply account for the self-sustaining lubricating boundary layers as the gel surface wears away. It is also consistent with the thickness of the lipid layer transferred to the metal surface indicated above (figs. 3B, C).

We show that trace incorporation of PC lipids provides a simple route to creating hydrogels that can continuously lubricate themselves as they wear, via the hydration lubrication mechanism attributed to PC-exposing boundary layers on articular cartilage. Such gels maintain very low friction and wear up to contact stresses of several MPa and sliding velocities up to cm/s, while minimally perturbing their bulk mechanical properties. Our approach may provide a platform for creating self-lubricating hydrogels wherever low friction and low wear are required.

References:

1. N. A. Peppas, J. Z. Hilt, A. Khademhosseini, R. Langer, Hydrogels in biology and medicine: from molecular principles to bionanotechnology. *Adv. Mater.* **18**, 1345-1360 (2006).
2. J. J. Green, J. H. Elisseeff, Mimicking biological functionality with polymers for biomedical applications. *Nature* **540**, 386-394 (2016).
3. M. Liu *et al.*, An anisotropic hydrogel with electrostatic repulsion between cofacially aligned nanosheets. *Nature* **517**, 68-72 (2015).
4. J. P. Gong, Friction and lubrication of hydrogels—its richness and complexity. *Soft Matter* **2**, 544-552 (2006).
5. A. A. Pitenis, J. Manuel Urueña, A. C. Cooper, T. E. Angelini, W. Gregory Sawyer, Superlubricity in gemini hydrogels. *J. Tribol* **138**, 042103 (2016).
6. X. Zhang, J. Wang, H. Jin, S. Wang, W. Song, Bioinspired supramolecular lubricating hydrogel induced by shear force. *J. Am. Chem. Soc.* **140**, 3186-3189 (2018).
7. J. Cui, D. Daniel, A. Grinthal, K. Lin, J. Aizenberg, Dynamic polymer systems with self-regulated secretion for the control of surface properties and material healing. *Nat. Mater.* **14**, 790-795 (2015).

8. E. Porte, P. Cann, M. Masen, Fluid load support does not explain tribological performance of PVA hydrogels. *J. Mech. Behav. Biomed. Mater.* **90**, 284-294 (2019).

9. W. C. Hayes, V. C. Mow, *Basic orthopedic biomechanics*. (Lippincott-Raven, Philadelphia, 1997).

10. H. Forster, J. Fisher, The influence of loading time and lubricant on the friction of articular cartilage. *Proc. Inst. Mech. Eng. H* **210**, 109-119 (1996).

11. S. Jahn, J. Seror, J. Klein, Lubrication of articular cartilage. *Annu. Rev. Biomed. Eng.* **18**, 235-258 (2016).

12. S. Lee, N. D. Spencer, Sweet, hairy, soft, and slippery. *Science* **319**, 575 (2008).

13. J. Seror, L. Zhu, R. Goldberg, A. J. Day, J. Klein, Supramolecular synergy in the boundary lubrication of synovial joints. *Nat. Commun.* **6**, 1-7 (2015).

14. W. H. Briscoe *et al.*, Boundary lubrication under water. *Nature* **444**, 191-194 (2006).

15. J. A. Buckwalter, H. J. Mankin, A. J. Grodzinsky, Articular cartilage and osteoarthritis. *Instr. Course Lect.* **54**, 465 (2005).

16. J. Klein, Repair or replacement: a joint perspective. *Science* **323**, 47-48 (2009).

17. G. D. Jay, K. A. Waller, The biology of Lubricin: Near frictionless joint motion. Matrix Biol. 39, 17-24 (2014)

18. A. Singh *et al.*, Enhanced lubrication on tissue and biomaterial surfaces through peptide-mediated binding of hyaluronic acid. *Nat. Mater.* **13**, 988-995 (2014).

19. M. K. Kosinska *et al.*, A lipidomic study of phospholipid classes and species in human synovial fluid. *Arthritis. Rheum.* **65**, 2323-2333 (2013).

20. A. Sarma, G. Powell, M. LaBerge, Phospholipid composition of articular cartilage boundary lubricant. *J. Orthop. Res.* **19**, 671-676 (2001).

21. B. Hills, B. Butler, Surfactants identified in synovial fluid and their ability to act as boundary lubricants. *Ann. Rheum. Dis.* **43**, 641-648 (1984).

22. R. Sorkin, N. Kampf, Y. Dror, E. Shimoni, J. Klein, Origins of extreme boundary lubrication by phosphatidylcholine liposomes. *Biomaterials* **34**, 5465-5475 (2013).

23. M. E. Freeman, M. J. Furey, B. J. Love, J. M. Hampton, Friction, wear, and lubrication of hydrogels as synthetic articular cartilage. *Wear* **241**, 129-135 (2000).

24. A. Hogt *et al.*, Wettability and ζ potentials of a series of methacrylate polymers and copolymers. *J. Colloid Interface Sci.* **106**, 289-298 (1985).

25. Q. Chen, D. Zhang, G. Somorjai, C. R. Bertozzi, Probing the surface structural rearrangement of hydrogels by sum-frequency generation spectroscopy. *J. Am. Chem. Soc.* **121**, 446-447 (1999).

26. L. Boulangé-Petermann, A. Doren, B. Baroux, M.-N. Bellon-Fontaine, Zeta potential measurements on passive metals. *J. Colloid Interface Sci.* **171**, 179-186 (1995).

27. A.-M. Trunfio-Sfarghiu, Y. Berthier, M.-H. Meurisse, J.-P. Rieu, Role of nanomechanical properties in the tribological performance of phospholipid biomimetic surfaces. *Langmuir* **24**, 8765-8771 (2008).

28. R. Goldberg *et al.*, Boundary lubricants with exceptionally low friction coefficients based on 2D close‐packed phosphatidylcholine liposomes. *Adv. Mater.* **23**, 3517-3521 (2011).

29. T. W. Carone, J. M. Hasenwinkel, Mechanical and morphological characterization of homogeneous and bilayered poly (2‐hydroxyethyl methacrylate) scaffolds for use in CNS nerve regeneration. *J. Biomed. Mater. Res. B* **78**, 274-282 (2006).

30. Z. Qu, H. Xu, H. Gu, Synthesis and Biomedical Applications of Poly ((meth) acrylic acid) Brushes. *ACS Appl. Mater. Interfaces* **7**, 14537-14551 (2015).

31. S. A. Angayarkanni, N. Kampf, J. Klein, Surface Interactions between Boundary Layers of Poly (ethylene oxide)–Liposome Complexes: Lubrication, Bridging, and Selective Ligation. *Langmuir* **35**, 15469-15480 (2019).

32. Y. Cao, N. Kampf, J. Klein, Boundary Lubrication, Hemifusion, and Self-Healing of Binary Saturated and Monounsaturated Phosphatidylcholine Mixtures⧫. *Langmuir* **35**, 15459-15468 (2019).

33. E. Sackmann, Membrane bending energy concept of vesicle‐and cell‐shapes and shape‐transitions. *FEBS Lett.* **346**, 3-16 (1994).

34. H. Duwe, J. Kaes, E. Sackmann, Bending elastic moduli of lipid bilayers: modulation by solutes. *J. Phys. France* **51**, 945-961 (1990).

35. E. P. Chan, Y. Hu, P. M. Johnson, Z. Suo, C. M. Stafford, Spherical indentation testing of poroelastic relaxations in thin hydrogel layers. *Soft Matter* **8**, 1492-1498 (2012).

36. H. Yu, S. Sanday, B. Rath, The effect of substrate on the elastic properties of films determined by the indentation test—axisymmetric Boussinesq problem. *J. Mech. Phys. Solids* **38**, 745-764 (1990).

37. J. Klein, Molecular mechanisms of synovial joint lubrication. *Proc. Inst. Mech. Eng. J* **220**, 691-710 (2006).

38. K. L. Johnson, *Contact mechanics*. (Cambridge University Press, London, 1987).

Acknowledgements: We thank Sam Safran and Annabel Butcher for useful discussions, and Michael Urbakh for comments on the ms. The electron microscopy studies were conducted at the Irving and Cherna Moskowitz Center for Nano and Bio-Nano Imaging at the Weizmann Institute of Science.

Funding: This project has received funding from the European Research Council (ERC) under the European Union's Horizon 2020 research and innovation programme (grant 743016). We thank the McCutchen Foundation, the Israel Science Foundation-National Science Foundation China (Grant 2577/17), the Israel Ministry of Science and Technology (Grant 713272) and the Weizmann-EPFL Collaboration Program funded by the Rothschild Caesarea Foundation, for support of this work. This work was made possible in part through the historic generosity of the Harold Perlman family.

Author contributions: RG and JK conceived the project; RG, WL, MK, NI and NK carried out experiments; ES and RG carried out the cryo-SEM imaging; JK, RG, WL and MK wrote the ms. and analyzed the data. All co-authors commented on the ms.

Competing interests: The Weizmann Institute has a patent on low friction hydrogels.

Data and Materials availability: All data are available in the manuscript or the supplementary material.

Supplementary content (references (*29* – *38*)) available with this paper includes a 'Materials and Methods' part with 11 sections, referred to in text as 'Methods sections 1 – 11'; and a 'Supplementary Discussion' part with 14 sections, referred to in text as '*SD*1 – *SD*14', incorporating 16 figures (figs. S1 – S16).

Figures:

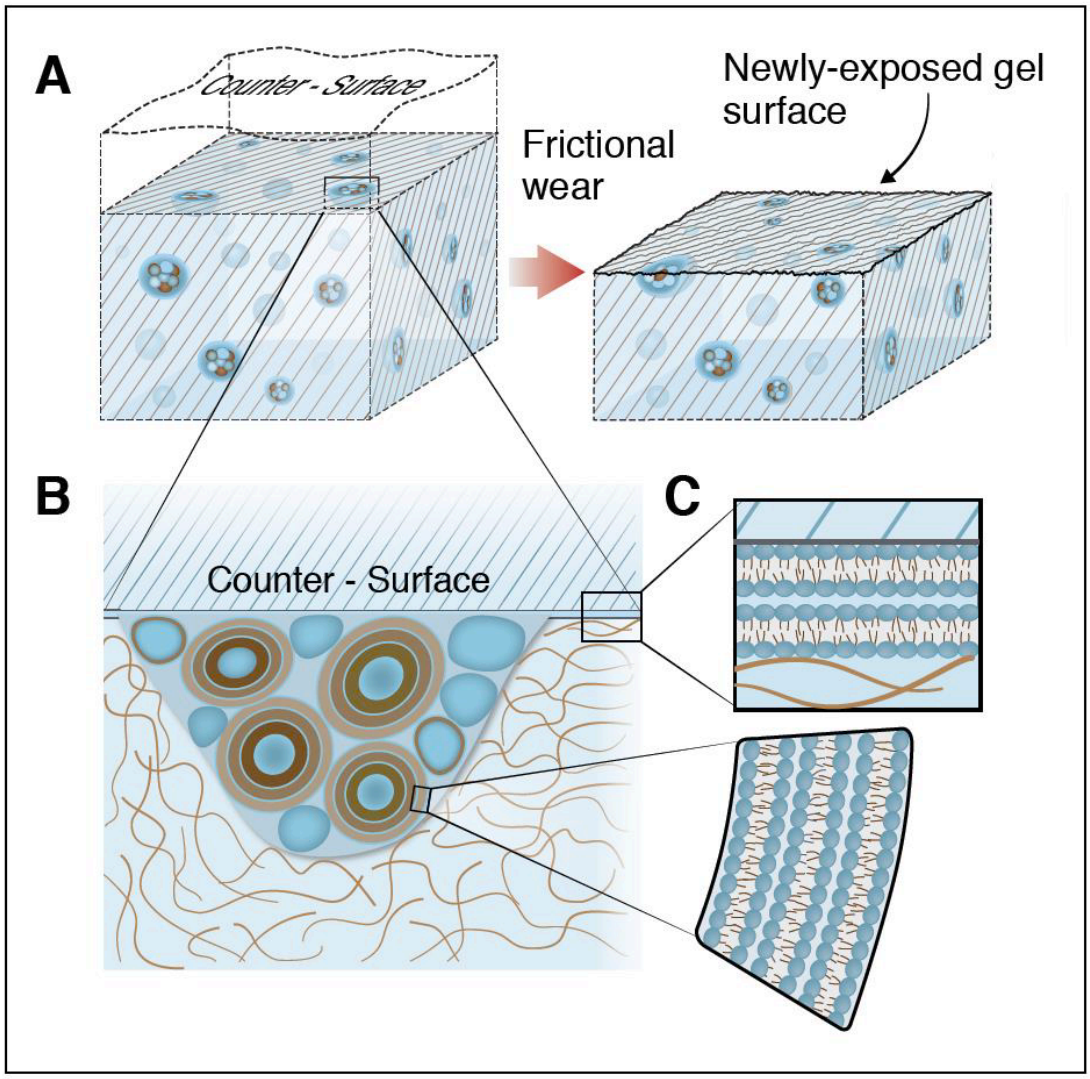

Fig. 1. Schematic illustrating the self-lubrication of lipid-incorporating hydrogels. As the surface of the hydrogel, incorporating lipids as vesicles in micro-reservoirs **(A)**, wears away due to friction, additional micro-reservoirs of lipid are exposed. This enables boundary layers of lipids to form on the surfaces **(B and C)**, leading to friction reduction via the hydration lubrication mechanism at the slip-plane between the highly-hydrated lipid headgroups.

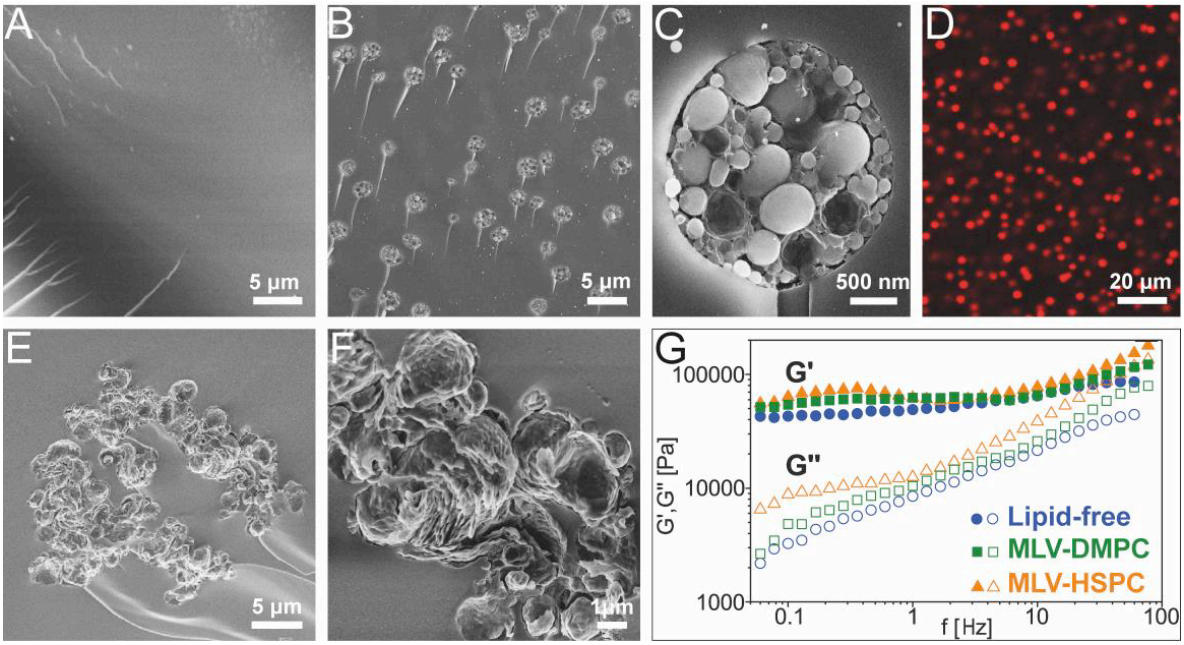

Fig. 2. Characterization of lipid-free and lipid-incorporating hydrogels. (A) Freeze fracture surface of lipid-free pHEMA hydrogel. **(B)** Freeze-fracture surface of the gel incorporating DMPC vesicles, showing the micro-reservoirs transected by the surface. **(C)** A single micro-reservoir from (B) at larger magnification. **(D)** Confocal microscopy section of the hydrogel incorporating fluorescently-labeled DMPC vesicles, showing the lipid micro-reservoir distribution. **(E)** Freeze-fracture surface of the gel incorporating HSPC vesicles. **(F)** Microreservoir from (E) at larger magnification. **(G)** Storage and loss moduli of lipid-free and lipid-incorporating pHEMA gels.

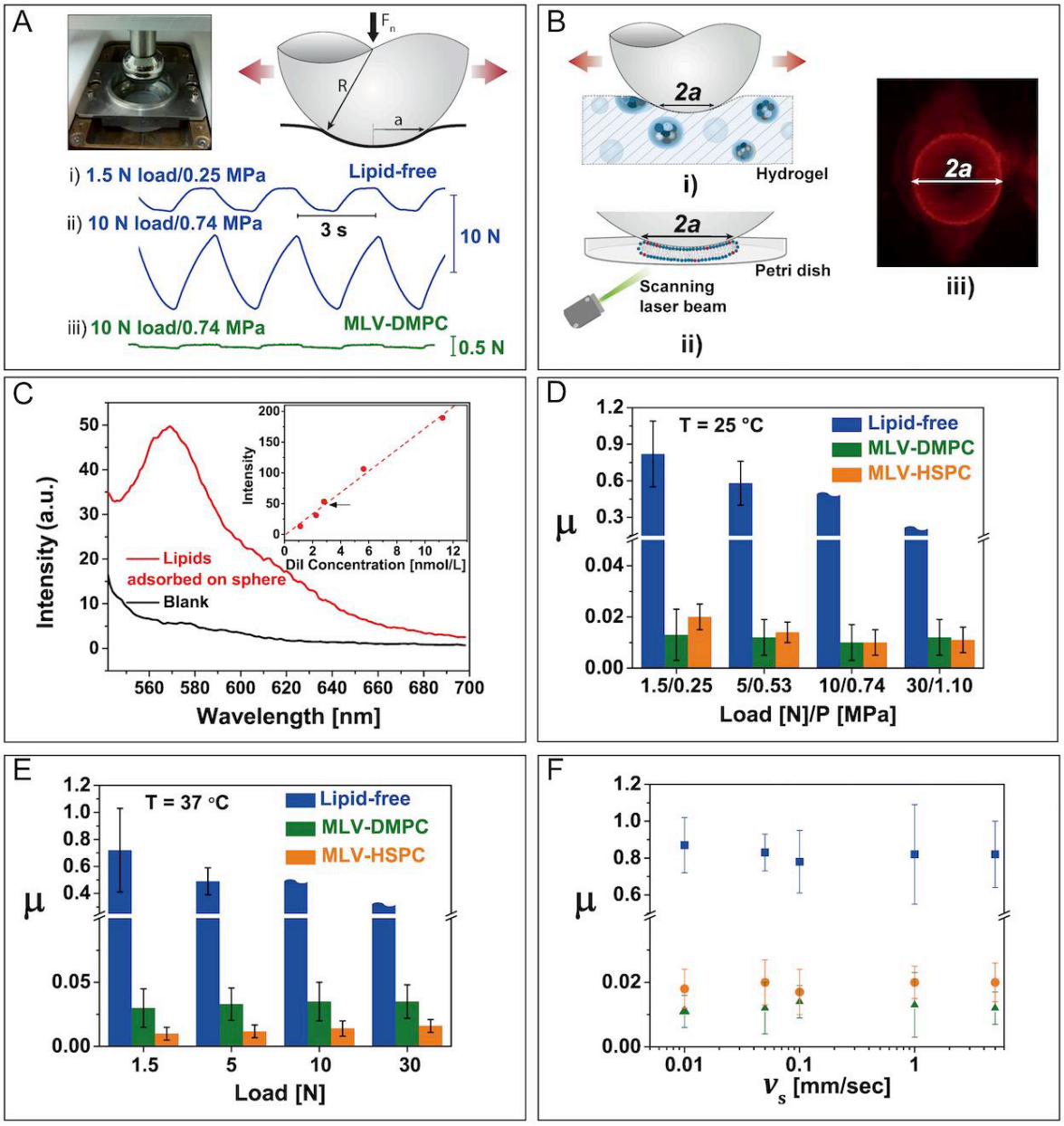

Fig. 3. Sliding between a steel sphere and pHEMA hydrogels. (A) Showing the UMT tribometer and sliding configuration (Methods, section 7), and typical friction vs. time traces for lipid free and lipid-incorporating gels, where F_s is taken as half the amplitude between sliding plateaus. The middle trace – no sliding plateau - indicates that sliding is not achieved, and that F_s must be larger than half the amplitude between peaks. **(B)** The transfer of fluorescently-labelled lipids incorporated in the gel to the contact area (radius *a*) with the sliding steel sphere, as in (i), is monitored as follows. The steel sphere following sliding is placed in a Petri-dish and the dye in the transferred lipid layer is excited with a

scanning laser beam as in (ii), and imaged with a photomultiplier tube to yield images as in (iii), which shows the lipid transfer following 5 mins sliding. The amount of transferred lipids is then quantified as in **(C)** (see also Methods, section 11). **(D)** and **(E)** show friction coefficient values μ at room and physiological temperatures respectively, at a series of loads and corresponding contact stresses. 'Wavy-topped' columns indicate that no sliding was achieved (see middle trace in (A)), so that μ must be larger than the column height shown. **(F)** Variation of μ with sliding velocity v_s for lipid-free (blue symbols) and lipid-incorporating pHEMA gels (HSPC – orange; DMPC – green).

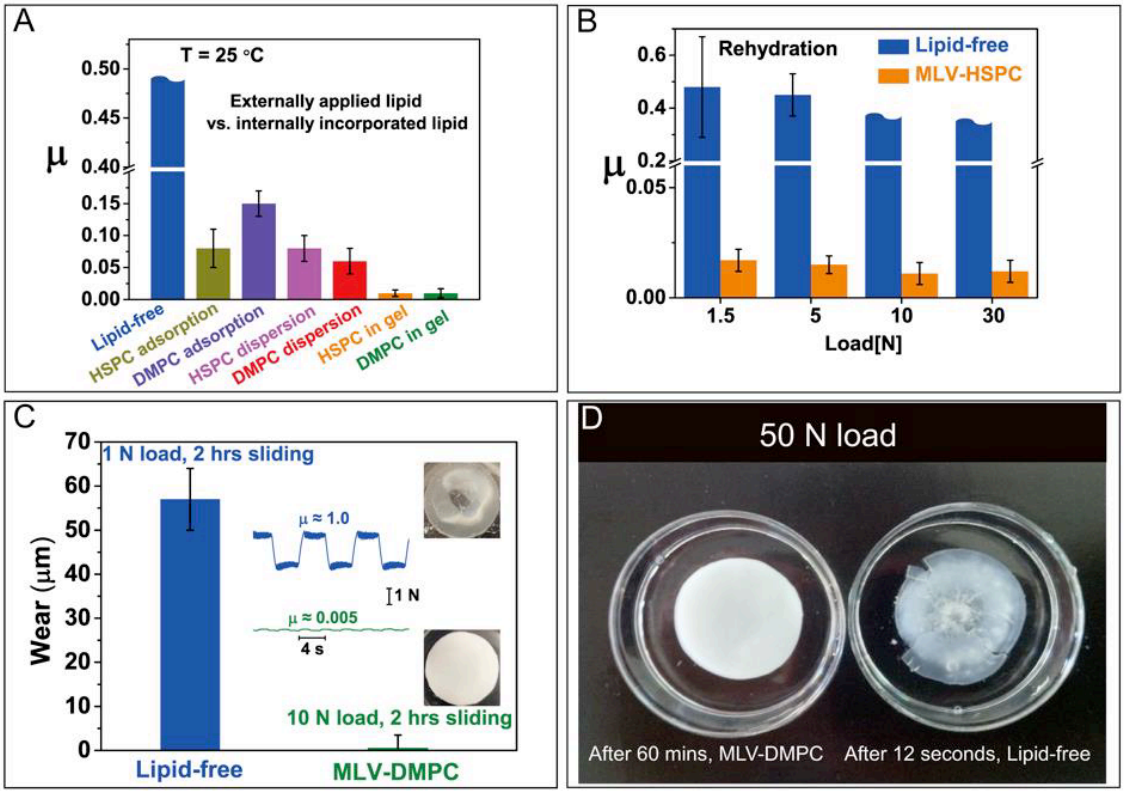

Fig. 4. Friction and wear of lipid-treated pHEMA gels. (A) Sliding friction between lipid-free gels (blue) and between lipid-free gels after adsorption of HSPC (olive green) and DMPC (violet) followed by washing, following 30 mins sliding; and between lipid-free gels immersed in lipid dispersions (purple and red), compared with lipid-incorporating gels immersed in water (orange and green). **(B)** The effect of rehydration following dehydration of lipid-free and HSPC-incorporating gels, showing the retention of the characteristic self-lubricating ability for the latter. **(C)** Wear of lipid-free and of DMPC-incorporating gels, showing typical friction traces as well as the visual appearance of the gel samples, following 2 hours sliding of the steel sphere on the gels, at 1 N load for the lipid-free gel and 10 N load for the lipid-incorporating gel. The wavy-topped columns represent a lower bound on μ, see also fig. 3 D & E and Methods section 7. **(D)** Appearance of gel samples under 50 N load (1.53 MPa contact stress) on the steel sphere, showing unchanged appearance following 1 hr sliding (corresponding to 9 μm wear) for a DMPC-incorporating gel, while the lipid-free gel was torn after 12 s of back-and-forth shear under the load.

Supplementary Materials for

Cartilage-inspired, lipid-based boundary-lubricated hydrogels

Weifeng Lin, Monika Kluzek, Noa Iuster, Eyal Shimoni, Nir Kampf, Ronit Goldberg, Jacob Klein

correspondence to: ronit.goldberg@lipo-sphere.com; jacob.klein@weizmann.ac.il

This PDF file includes:

Materials and Methods

Contents

1. Materials

Water used was purified using a Barnstead NanoPure system (ThermoFisher Scientific, Waltham, MA, USA) to 18.2 MΩ cm resistivity and total organic content < 1 ppb (henceforth 'purified water'). 1,2-dimyristoyl-sn-glycero-3-phosphatidylcholine (DMPC) and hydrogenated soy phosphatidylcholine (HSPC) lipids were purchased from Lipoid, GmbH (Germany). 2-hydroxyethyl methacrylate (HEMA), ammonium persulfate (APS), *N,N,N′,N′*-tetramethylethylenediamine (TMEDA), ethylene glycol dimethacrylate (EGDMA, with either 1 or 9 EG units), and 1,1′-Dioctadecyl-3,3,3′,3′-tetramethylindocarbocyanine perchlorate (DiI) were purchased from Sigma-Aldrich (Israel) and used as received. 8-hydroxypyrene-1,3,6-trisulfonic acid, trisodium salt (HPTS) was purchased from ThermoFisher Scientific (Waltham, MA, USA).

2. Liposome preparation and size characterization

Multilamellar vesicles (MLVs) composed of DMPC and HSPC were prepared by sonicating the lipids in water for 15 mins at 30 °C and 60 °C respectively (ca. 5 °C above the respective lipid solid-ordered to liquid-disordered transition temperatures) to a final dispersion concentration of 45 mM. Dynamic light scattering (Viscotek 802 DLS, Malvern Instruments, UK) from a 1 mM dispersion of the lipids was used to characterize their size distribution. The DLS data showed that the MLV-DMPC liposomes had three main peaks at diameters 35±5 nm, 122±15 nm and 570±80 nm, while MLV-HSPC liposomes had a single peak at diameter 540±100 nm.

3. Hydrogel preparation

Lipid-free pHEMA hydrogels as used in this study were prepared as follows (*29*): HEMA (3 mL = 24.6 mmol), EGDMA (generally 0.095 mL = 0.5 mmol, though other cross-linker concentrations could also be used, see below), APS aqueous solution (0.2 mL containing 0.105 mmol APS), and purified water (2 mL) were added together and vigorously stirred for 0.5 hour. The molar ratio of the EGDMA cross-linker to the HEMA monomer was thus generally 2% (but could be varied between 4% and 0.1%, see e.g. *SD*9). TMEDA (50 μL) was added to the mixture (to accelerate the reaction), which was then stirred for 20 seconds and poured into a 6 cm diameter petri dish. The mixture was allowed to gel at room temperature for 4 hours, followed by immersion in a large excess of purified water for 3 days to remove unreacted materials. This resulted in very slight swelling of the pHEMA hydrogels, whose final water content was measured at 38.3±0.3% of the gel weight (determined by weighing after oven-drying to constant

weight). The hydrogels thus obtained were cut into circular disks of diameter 20 mm and measured thickness ~2 mm suitable for tribological and other characterizations, where the surface exposed to air during the gelation was used for the friction measurements. Liposome-incorporating gels were prepared similarly save that the 2 mL purified water was replaced by 2 mL of the respective MLV dispersion at concentration 45 mM. This corresponds to a volume fraction ϕ of lipids in the hydrogel $\phi \approx 0.012$ (DMPC) or $\phi \approx 0.014$ (HSPC).

4. Rheometry

Viscoelastic measurements were performed using a strain/stress-controlled rheometer (Thermo-Haake, Mars III, Karlsruhe, Germany). Samples were prepared in the form of disks with a diameter of 20 mm and thickness ~2 mm. Samples were tested using a parallel plate geometry. The samples were placed between the rheometer plates and a slight compression of ~0.8 N was applied. Amplitude sweep tests were performed in constant strain mode for strains in the range of 10^{-4} to 0.5, the oscillation frequency being 1 Hz. Frequency sweep tests were performed in stress control mode, with stress being in the range of the linear viscoelasticity, as determined from the amplitude sweep studies. The frequency range was typically between 0.05 and 30-100 Hz.

5. Cryo-SEM freeze fracture imaging

Hydrogel samples were sectioned to slices of thickness 100 μm using a vibratome (Electron Microscopy Sciences, USA). The slices were sandwiched between an aluminum disc with a depression of depth 150 μm and a flat disc (M. Wohlwend GmbH, Switzerland) and were then cryo-immobilized by high pressure freezing (HPM010, Bal-Tech, Liechtenstein). The frozen sample was removed from the disc under liquid nitrogen, mounted perpendicularly in a holder, transferred to a BAF 60 freeze fracture device (Leica Microsystems, Austria) using a VCT 100 cryo transfer shuttle (Leica) and was fractured perpendicularly to the plane of the frozen slice at -120 °C under a pressure of about $5x10^{-7}$ mbar. The cold fractured surface was sometimes "etched" by increasing the temperature to about -105 °C for several minutes to let some frozen water sublime. The fractured sample was then transferred to an Ultra 55 cryo-scanning electron microscope (Zeiss, Germany) and observed using an InLens Secondary electrons detector at an acceleration voltage ranging between 1-2.5 kV.

6. Confocal fluorescence microscopy imaging

To prepare DMPC MLV-incorporated hydrogels for confocal fluorescence microscopy imaging, hydrogels were prepared as above (section 3) save that the 2 mL purified water was replaced by 2 mL MLV-HSPC incorporating 0.02 mol% of DiI (MLV-DMPC-DiI), which was prepared as follows. DMPC (457 mg = 0.67 mmol) and DiI (0.12 mg = 0.13 μmol) were dissolved in chloroform (3 mL). The chloroform was removed by purging in nitrogen overnight, and the MLV-DMPC-DiI was prepared by sonicating the lipid-DiI in water at 30 °C for 15 mins.

Confocal pictures were acquired using a customized IX83 spinning disk confocal microscope (Olympus Life Science, Olympus Co., Japan), equipped with an iXON IX83P camera (Andor, UK). Laser illumination for the DiI-stained liposomes and HPTS, present in the bulk solution to detect the hydrogel interface, was achieved using solid-state VS-LMS diode lasers (Visitron Systems GmbH, Germany), using 560 nm and 488 nm excitation wavelengths, respectively. Both excitation lasers were used at 53 mW power and 100 ms exposure time. All images were acquired using a 40×, oil immersion PLANAPO objective (NA 1.2), with a 0.3 μm optical slice step for z scanning. Picture analysis was performed using ImageJ software v1.52i (NIH, USA).

7. Friction measurements

Friction measurements, based on several independent experiments (different hydrogel samples with at least 2 different contact points on each sample) for each set of conditions, were carried out using a CETR UMT tribometer (Bruker, MA, USA) with normal and friction force sensors as well as a capacitance-based sensor to determine wear and to determine the indentation depth δ of the hydrogel corresponding to each load (see also *SD*11). Measurements were in all cases carried out under high-purity water unless stated. The friction force F_s between the pHEMA hydrogel and the polished stainless-steel spherical head (diameter 22 mm), configuration as in fig. 3A, was measured at different sliding velocities v_s and loads F_n (as shown in figs. 3 and 4) corresponding to different mean pressures $P = (F_n/A)$ over the contact area A. $A = \pi a^2$ was evaluated from the measured indentation δ of the gel surfaces under the steel sphere at different loads (fig. 3A), where the contact radius a was determined using an approach based on numerical

calculations for the case where the thickness h of the indented gel is comparable to or less than a (*SD*12). Loads used were generally in the range 1.5-30 N and occasionally higher as shown in fig. 4 – up to the breaking point of the hydrogel. F_s was determined (generally over a 5 min back-and-forth sliding time) from its value in the plateau region of the friction traces (fig. 3A), and friction coefficients evaluated at each load as $\mu = F_s/F_n$. Where sliding (and thus a plateau in the traces) could not be achieved due to the friction exceeding the maximal applied shear force $F_{shear,\ max}$ between steel surface and hydrogel (an example is shown in the trace (ii) of fig. 3A), or due to the hydrogel tearing under the load and applied motion, the friction coefficients are indicated, by wavy-topped columns in figs 3 and 4, as being larger than ($F_{shear,\ max}/F_n$). The magnitude of the measured sliding friction, both for lipid-free and lipid-incorporating gels, could vary by up to ca. 2-fold between different gel samples for a given configuration (load, temperature and nature of the gel), attributed to slight differences in surface morphologies of the gel samples arising from small variations in the casting conditions.

8. Externally applied lipids

Two experimental configurations were used, one where the lipid-free hydrogels were immersed in a liposomes dispersion then then rinsed prior to friction measurements in water; the other where the friction was measured in a liposome dispersion. In the first case, lipid-free hydrogels were immersed in MLV-DMPC or MLV-HSPC dispersions (45 mM) for 3 hours followed by overnight immersion in a large excess (250 mL) of purified water to remove excess dispersion; subsequent friction measurements were carried out under water, and μ values (fig. 4A) are shown after 30 mins of back and forth sliding (see Extended Information for effect of sliding time on μ). In the second case, friction

measurements were carried out on the lipid-free hydrogels immersed in either MLV-DMPC or MLV-HSPC suspensions (45 mM).

9. Dehydration/Rehydration Protocol

HEMA hydrogels were dried by heating in an air-oven to 60 ºC until hydrogels were completely dry as determined by progressive weighing till no further weight loss was recorded. Subsequently the dried hydrogels were rehydrated by immersion in purified water for 3 days when they regained their original water content (determined by weighing), and sliding friction was then re-measured in the tribometer.

10. Estimating the amount of lipids available at a wear-exposed hydrogel surface

As the hydrogel surface wears, new surfaces are progressively exposed. Each such surface will transect randomly-distributed micro-reservoirs of the lipids as indicated in fig. 1 and figs. 2B,C (for definiteness, we relate to the gel-incorporated DMPC lipids), and the lipids in these transected reservoirs will be available to coat the surfaces of the gel and the counter-surface sliding past it (fig. 1). Here we evaluate this availability. Any plane in the gel that is within a distance R_0 of the centre of a spherical reservoir (of radius R_0) will transect it and so have access to the liposomes within. The number of such transected reservoirs per area A of the plane is $A\rho_{2D}$, where ρ_{2D} is the number of transected-reservoirs/unit-area. This equals the number of reservoirs whose centre is within a volume $2AR_0$ (since reservoirs can be either side of the plane), and for a number density ρ_{3D} of reservoirs per unit volume of the gel, we then have $A\rho_{2D} = 2AR_0.\rho_{3D}$, i.e.

$$\rho_{2D} = 2R_0.\rho_{3D} \quad \text{(M1)}$$

If v is the volume of lipids within each reservoir, then the volume fraction ϕ (<< 1) of lipids in the gel is given by

$$\phi \approx v.\rho_{3D}. \quad \text{(M2)}$$

The total volume of lipids $V_{lipids/area}$ available to coat unit area of the gel surface and the counter-surface is just the volume of lipids in the transected reservoirs,

$$V_{lipids/area} = v.\rho_{2D}. \quad \text{(M3)}$$

We thus have, from eqs (M1 - 3),

$$V_{lipids/area} \approx 2R_0\phi \quad \text{(M4)}$$

As this is the total volume of lipids accessible per unit area of the interface from the truncated micro-reservoirs, it is also the maximal thickness d of the lipid layer that is available to coat the two opposing interfaces, as stated in eq (1) of the main text.

11. Fluorescence-based monitoring of gel-to-metal transfer of lipids during sliding

Lipid transfer via metal-gel sliding and imaging of transferred lipids

The spherical steel head (section 7 above) was slid past pHEMA hydrogels incorporating DMPC-MLV stained with 1% DiI, at sliding velocity 1 mm/s for 5 min. It was then placed in a petri dish (fig. 3B(ii)) and the area of absorbed lipids transferred during the sliding was imaged (fig. 3B(iii)) by excitation of DiI dye at 532 nm using a Typhoon FLA 9500 scanner (GE Healthcare Bio-Sciences AB, Sweden), with photomultiplier tube set up at 500× gain and pixel size 50 µm. Subsequently the head was washed with ethanol, dried, and visualized again in order to confirm lack of fluorescence after removal

of lipids, while the amount of lipids in the ethanol was assayed as below. Pictures were analyzed using ImageJ software (NIH, USA).

Assay of lipids transferred from gel to steel surface

Following removal of the transferred lipids from the steel sphere by ethanol as above, the solvent was evaporated under a nitrogen stream, and left overnight under vacuum. 400 μL of chloroform was used to re-suspend the lipids, and the solution was placed in a quartz silica cuvette with a 1 mm path length. Acquisition of DiI emission spectra was performed with an Agilent Cary Eclipse Fluorescence Spectrophotometer (Varian Instruments, Walnut Creek, CA) at room temperature. The excitation wavelength was set at 500 nm with a bandpass of 20 nm, and the emission was also recorded with bandpass of 20 nm. Spectrum acquisition was repeated over 3 separate samples; a typical spectrum is shown in fig. 3C. A calibration curve (inset to fig. 3C) was prepared by measuring the maximal fluorescence intensity of known amounts of pure DMPC-DiI-chloroform solution by the same method and parameters to ensure the same experimental conditions. By comparing the maximal fluorescence intensity of the lipids transferred to the metal (arrow in inset to fig. 3C) the amount of transferred lipid could then be determined, and from the known area πa^2 of the transferred lipid film (fig. 3B(iii)) the mean film thickness could be evaluated.

Supplementary Discussion

Contents

9. Effect on friction of varying the pHEMA gel modulus
10. Variation of micro-reservoir size with lipid concentration in pHEMA gel
11. Wear vs. time traces
12. Mean contact stresses between sphere and hydrogel
13. Concerning wear of the lipid-incorporating pHEMA hydrogel under sliding
14. Concerning affine conformation of hydrogel surfaces by compressed counter-surfaces

1. Lipid incorporation in different hydrogels

In addition to the relatively low water-content (ca. 40% water), relatively high-modulus pHEMA gel described in the main text, the effect of PC-lipid-incorporation on friction was examined in different hydrogels (as shown in fig. S1). DMPC lipids were incorporated, at concentrations in the range 16-24 mg/mL, in a number of other hydrogels with higher water content and correspondingly lower moduli than the pHEMA gel. Preliminary friction measurements - on two separate gel samples in each case, with two contact points per sample – were carried out in the same steel-sphere-sliding-on-gel configuration as in fig. 3A (main text). Gels used were

A) Polymethacrylamide hydrogel (PMAM; 2% poly(ethylene oxide) dimethacrylate crosslinker; water content 66±2%; modulus $G' \approx (6\pm2) \times 10^4$ N/m^2).

B) Poly(HEMA-co-methacrylic acid) hydrogel (PHM; 0.75% EDGMA crosslinker; water content 83±2%; modulus $G' \approx (4.5\pm1) \times 10^3$ N/m^2)

C) Poly(acrylic acid-co-dimethacrylamide) hydrogel (PDA; ~0.55% EDGMA crosslinker; water content 98%; modulus G' ca. 780 N/m^2

D) X-linked gelatin methacrylate hydrogel (PGM; water content 84±2%; modulus $G' \approx (6\pm2) \times 10^3$ N/m^2).

We emphasize the preliminary nature of these measurements; nonetheless they show that for these hydrogels, which differ significantly from the pHEMA gel of the main paper, incorporation of a low DMPC concentration reduces greatly the friction coefficient relative to the lipid-free gel. In the case of the PMAM hydrogel we also examined the effect of incorporating HSPC to a similarly low concentration (20 mg/mL): as shown in fig. S2, a similar reduction in the friction coefficient is provided by the incorporated HSPC lipids to that afforded by the incorporated DMPC. Attachment of the liposomes to the PHM and PDA hydrogels, which are negatively charged (*30*) is attributed to dipole-charge interactions similarly to the negatively charged pHEMA hydrogel in the main text. In the case of the neutral PMAM and to PGM hydrogels, the attachment of the PC lipids is attributed to zwitterionic-dipole/induced-dipole attraction, as seen in the attachment of PC lipids to other neutral polymers such as PEO (*31*).

2. Effect of sliding time on lubrication of pHEMA hydrogel by adsorbed lipids

Lipid-free pHEMA hydrogels that had been immersed in DMPC and HSPC liposome dispersions and then washed (Methods section 3) prior to friction measurements, showed initially lower friction but these rapidly increased with measurement time (in contrast to friction measurements for either lipid-incorporated hydrogels or lipid-free hydrogels measured in liposome dispersions, fig. 4B in main text, where the friction did not change with measurement time). This is shown in fig. S3, where the initial friction (time t = 0) increased substantially following t = 30 mins sliding. This is attributed to wear and

removal, with no replenishment possibility, of the initial adsorbed boundary lubricating layer.

3. AFM of liposomes adsorbed on the polished steel head and on a pHEMA-coated surface.

In addition to the fluorescence imaging and assay of lipids transferred to the steel sphere during rubbing of the gel (fig. 3B, C in main text), we examined via atomic force microscopy (AFM) imaging whether PC liposomes adsorb to the polished stainless steel spherical head used in our friction experiments (fig. 3A), and to a substrate coated with pHEMA. For the steel head we further examined the adsorption on the steel head following its rubbing on the pHEMA hydrogel surface using fluorescence measurements (below). Imaging was with a Molecular Force Probe 3D AFM (MFP 3D^{TM}, Oxford Instruments Asylum Research, Santa Barbara, CA). The steel surface was incubated for 3 hours under water, or under an MLV suspension (10-100 μM) of either DMPC or HSPC. Tapping-mode scanning was carried out (under liquid) using a silicon tip (SNL, Bruker Nano Inc, USA) with V-shaped nitride lever having a nominal spring constant of 0.35 N/m. Images are shown in fig. S4(a) – (c). They reveal the adsorption of the DMPC onto the steel surface, where the liposomes rupture to form bilayers (as seen previously on bare mica (*22*)), and of the adsorption of HSPC onto the steel surface in the form of quasi-spherical vesicles.

For the case of liposomes adsorbed on a pHEMA coated surface: freshly cleaved mica surfaces were incubated overnight in pHEMA polymer (Mw ≈ 20,000 Da) solution in

water. Separate surface force balance measurements showed that the pHEMA adsorbed onto the mica to a hard-wall thickness of ca. 5 nm. The pHEMA coated mica surfaces were then incubated overnight in dispersions of single unilamellar vesicles (SUVs) of either DMPC or HSPC, prepared in the standard way via extrusion through membranes (*22*), then washed and imaged both in the AFM (all samples) and via cryo-scanning electron microscopy (the lipid-incubated samples). Images are shown in fig. S5 A – C. These show the adsorption of both lipids onto the pHEMA coated surface, with the HSPC seen as spherical vesicular forms, while the DMPC vesicles rupture to form bilayers (as for their adsorption on the steel surface, fig. S4(b) above, and bare mica (*22*)).

4. Confocal microscopy section through pHEMA hydrogels incorporating DMPC vesicles

Confocal microscopy was used as described in Methods (section 6) to image pHEMA hydrogels incorporating DiI-labelled DMPC vesicles, as shown in fig. S6.

5. Mechanism of spreading of lipids on the surfaces

The mechanism for the spreading of lipids on the gel due to the sliding of the counter-surface is attributed to the shear arising from the sliding, which extracts and spreads the lipids from surface-exposed micro-reservoirs onto the sliding surfaces. This is demonstrated directly as follows:

a) We incubated a gel incorporating DMPC micro-reservoirs (over which no sliding had occurred) for 20 mins in a solution of lipophilic DiI dye, a dye which fluoresces when in the hydrophobic tail domain of lipid bilayers. We then acquired images of the hydrogel using fluorescence confocal microscopy in *z*-scan mode, which allows acquiring pictures at incremental *z*-positions (focal planes). We subsequently measured the DiI fluorescence intensity at the gel surface by performing a 3D reconstruction of the field of view and plotting the intensity profile in the *z*-axis. We repeated this with a similar gel over which the steel sphere was slid for 5 minutes, measuring the fluorescence intensity in the region of the sliding contact. The results, shown below in fig. S7, reveal a much higher fluorescence intensity over the region where sliding took place. Since DiI only fluoresces when incorporated in the lipid bilayer, and the microscope acquisition parameters were kept constant for both samples, this shows directly that sliding is the driving mechanism for lipid layer formation on the gel surface from the micro-reservoirs.

b) In a related measurement, the stainless steel sphere was pressed for 5' without sliding on a pHEMA gel incorporating DiI labelled (fluorescent) DMPC lipid micro-reservoirs, and any transferred (fluorescing) lipids were imaged in a confocal microscope, and also isolated and examined spectroscopically (as in fig. 3B and 3C of main text). On a similar hydrogel sample the steel sphere was pressed and then slid across the surface for 5', and any lipids transferred to the sphere were similarly examined. The results, fig. S8, show that only when the sphere slides past the gel are lipids transferred to it, supporting the attributed mechanism.

6. Slip plane between lipid layers

Slip between lipid bilayers can in principle occur at the headgroup-headgroup interface or at the tail-tail interface. The reason why the slip plane is at the head-head rather than the tail-tail plane is because friction at the latter plane is much higher, and the system slips naturally, via hydration lubrication, at the plane (head-head) offering the lowest resistance to sliding. This is most directly seen in the recent study "Boundary Lubrication, Hemifusion and Self-Healing of Binary Saturated and Monounsaturated Phosphatidylcholine Mixtures", by Cao et al. (*32*). In this paper, especially figs. 4 and 5, it is shown that when hemi-fusion of two phosphatidylcholine (PC) bilayers sliding past each other occurs, so that the easy-sliding interface at the head-head plane is replaced by the high-friction tail-tail plane, the friction immediately increases so that sliding stops. These figures are reproduced in part below in fig. S9, illustrating why low-friction slip in our system occurs at the head-head and not at the tail-tail planes.

7. Lubrication with different counter-surfaces

Additional counter-surfaces (other than the polished stainless steel sphere in the main ms.), were examined, namely: glass; and a lipid-incorporating pHEMA hydrogel. The results are shown below in fig. S10, and reveal the friction reduction effect also with these different counter-surfaces, both very different to stainless steel.

8. Access of liposomes in dispersion into interfacial contact region

The reason for the poorer access of the lipids from the surrounding dispersion into the

inter-surface region between the lipid-free gel and the counter-surface may be understood quantitatively as follows. The liposome dispersion is in the form of DMPC vesicles, mostly multi-lamellar vesicles (MLVs), with only a very small concentration of free lipids in solution, at the critical micelle concentration, which is of order 6 nM for DMPC. Thus the lipids available to coat the surface are essentially all in the form of liposomes. These vesicles, whose diameter $D = 2R$ is of order a few hundred nanometers to a few microns (and in the case of the MLVs will consist of several smaller vesicles nested within a larger one), may readily access the free unconfined gel surface and adsorb onto it. However, in order for such a lipid vesicle to access the highly-confined region of contact between the steel sphere counter-surface and the gel over which it is sliding, with a thickness $2h$ of order 10-30 nm (the thickness of a few lipid bilayers), the vesicle needs to be severely distorted. This will cost considerable energy, $\Delta E_0(h)$ say, which we may evaluate as follows: $\Delta E_0(h)$ arises from the distortion of the liposome from a sphere of diameter D to a 'pancake' of thickness $2h$, and can be written as (*33*):

$$\Delta E_0(h) = \int \kappa c^2 dA \qquad (1)$$

where κ is the bending or rigidity modulus of the lipid vesicle, c is the local mean curvature of the vesicle membrane and the integral is over the area of the 'pancake'. Taking the pancake to be a flat disk of height $2h$ and radius R, where $h << R$, we have $c \approx (1/h)$ in an annulus of radius R at the disk edge, and zero elsewhere, giving $\Delta E_0(h) \approx 2\pi^2\kappa(R/h)$. Putting in values for DMPC vesicles of $\kappa \approx 10^{-19}$ J (*34*), taking $R = 200$ nm (say), and $h = 10$ nm, we find that $\Delta E_0(h) \approx 4 \times 10^{-17}$ J $\approx 10^4$ k_BT, where k_B is Boltzmann's constant and T the absolute temperature. The actual distortion energy of a DMPC-MLV to such a flat configuration is likely to be even higher, since we ignored the fact that MLVs contain multiple vesicles that all need to be distorted, and have taken a

rather small value for the size $2R$ of an MLV. This distortion energy $\Delta E_0(h)$ to squeeze the liposomes into the narrow gap ($2h$) between the steel and gel surfaces is far larger than any adsorption energy of the MLVs on the free gel surface, which arises from weak dipole-charge interactions and particularly counterion-release effects (and, given the zeta-potential of the pHEMA surface of order -10 mV, will be of order 10-100 k_BT depending on the MLV size). This tells us that as the counter-surface slides across the gel it will repel and dislodge from the surface any adsorbed liposomes in its way, and very few if any vesicles will be able to access the inter-surface gap. As a result, lipids that have been worn away by the friction will not be replenished, and thus the friction rises.

This explanation is further tested directly by the following experiment: the steel sphere was made to slide under load across a lipid-free pHEMA gel immersed in a DMPC-MLV dispersion for 0.5 h, following which the surfaces were separated for 5 mins, then again loaded and made to slide. The resulting friction (after 1 min sliding) was substantially reduced (and increased again, after 30 mins sliding, to its earlier value), as shown in fig. S11 below. This demonstrates directly that when the lipids originally coating the surface had been worn away (after 30 mins sliding), and the friction had risen, new lipids could not enter the contact area and provide good lubrication (due to confinement effects as noted above) until the surfaces were separated. The same effect does not apply when lipids are incorporated within the gel, as they are then replenished continuously at the contact area from the surface-exposed micro-reservoirs.

9. Effect on friction of varying the pHEMA gel modulus

Measurements were carried out on pHEMA hydrogels cross-linked to different extents,

and thus with different moduli (measured with rheometer). The friction coefficient is significantly higher at lower crosslink densities and correspondingly lower moduli, as shown in fig. S12. This arises, as noted in the ms., from additional sliding-friction dissipation pathways related to viscoelastic losses in the hydrogel.

10. Variation of micro-reservoir size with lipid concentration in pHEMA gel

The diameter of micro-reservoirs in the lipid-incorporating pHEMA gel could be varied systematically by incorporating different lipid concentrations, as shown in fig. S13.

11. Wear vs. time traces

Wear is measured in the UMT tribometer via a high-resolution air-gap capacitor which monitors vertical motion of the upper surface as it is slid laterally past the lower surface. For the 50 N load configuration shown in fig. 4D, the wear vs. time trace is shown in fig. S14 below.

12. Mean contact stresses between sphere and hydrogel

The mean contact stress $P = F_n/A$, where F_n is the applied load and A the contact area. Hertzian contact mechanics could not be applied in our case as the gel thickness is insufficient to apply the usual Hertzian rigid-sphere-vs.-elastic-half-space relations. Instead we utilized a numerical-method-based treatment, following the study by Chan et al. (*35*), which is based in turn on numerical calculations by Yu and co-workers (*36*), for spherical indentation geometry as shown in fig. S15 below.

For the case where the indentation is δ as shown, and the contact radius *a* is comparable with or larger than the gel thickness *h*, it may be written as

$$a = \sqrt{R\delta}\,.\,f_a(\sqrt{R\delta}\,/\,h) \qquad (2)$$

The first term on the RHS is the Hertzian contact radius ($(R\delta)^{1/2}$) valid for a semi-infinitely thick gel ($h \Rightarrow \infty$), while the function $f_a((R\delta)^{1/2}/h)$, which was solved numerically based on the work of Yu and co-workers (*36*), accounts for the deviations from Hertz mechanics arising from the finite gel thickness *h*. Its approximate analytical form (which fits closely the numerical calculations), taken from eq.(5) in ref. (*35*), is:

$$f_a(\sqrt{R\delta}\,/\,h) = \frac{1.41(\sqrt{R\delta}\,/\,h)^2 + 0.57(\sqrt{R\delta}\,/\,h) + 0.5}{(\sqrt{R\delta}\,/\,h)^2 + 0.49(\sqrt{R\delta}\,/\,h) + 0.5} \qquad (3)$$

The thicknesses *h* of our gel samples as made, as well as the extent of indentation δ at each load were recorded, and from the known radius *R* we evaluated $f_a((R\delta)^{1/2}/h)$ and thus *a*, and hence $A = \pi a^2$ and the mean contact stress *P*. Values of *P* appearing in the main text were calculated using this approach.

13. Wear of the lipid-incorporating pHEMA hydrogel under sliding

For sliding on the lipid-incorporating pHEMA gel at moderate loads (though still at contact stress of several atmospheres), the data indicate that the gels can sustain a large number of sliding cycles with low resulting wear. Thus (fig. 4C in main text) the pHEMA wear under 1 kg. load (10 N) is $\lesssim$ 3 mm after 2 hours back-and-forth sliding (4,800 back-

and-forth cycles, each of amplitude 3 mm, at sliding velocity 2 mm/sec). Since the sliding amplitude is comparable to or larger than the contact radius, the entire contact area is subject to wear following each back-and-forth motion. The mean wear per cycle over the contact area, w, is then given by $w = x/y$, where $x \lesssim 3$ mm is the total mean wear over the contact area, and $y = 4800$ is the number of back-and-forth passes, over the 2 hours of sliding. Thus $w \approx 6$ Å or less per pass. This implies that, under such a load, more than 1.5×10^6 back-and-forth motions would be required to wear down 1 mm of the lipid-incorporating pHEMA gel. Even at higher loads, such as shown in fig. 4D, where the load is 50 N (contact stress ca. 1.5 MPa), the wear is $x = 9$ mm (fig. S14), and $y = 2400$ back-and-forth passes after an hour of sliding, the wear w for each pass of the steel counter-surface over the contact area is only ca. 4 nm.

14. Affine conformation of hydrogel surfaces by compressed counter-surfaces

Suppose a non-smooth gel surface (schematically presented as an array of bumps each of radius R as shown) to be compressed with a contact stress P against a counter-surface (assumed much harder than the gel) as indicated schematically in fig. S16 (adapted from (*37*)).

Each of the 'bumps' of radius R and modulus (of the gel) K, will be flattened to a radius r as indicated on the RHS. From Hertzian contact mechanics (38) and for the counter-surface on the bottom having a modulus much larger than K, we expect $r^3 \approx (FR/K)$, where F is the normal load per bump corresponding to the normal contact stress P. Since $F \approx \pi R^2 P$, this gives $r \approx (\pi P/K)^{1/3} R$. Since r cannot exceed R, the condition $r \geq R$

indicates full flattening of the bump, i.e. conforming affine contact between the rough, soft gel and a hard counter-surface. This indicates that for $P \gtrsim (K/\pi)$ a rough gel surface conforms affinely to the hard counter-surface with which it is in contact. Since most gel moduli are typically 10^5 N/m^2 or less (e.g. fig. 2G in main text and also *SD* 1), this suggests that already at pressures as low as ca. 3×10^4 N/m^2 $\approx$ 0.3 gels will be in conformal contact with a compressing surface.

Fig. S1.

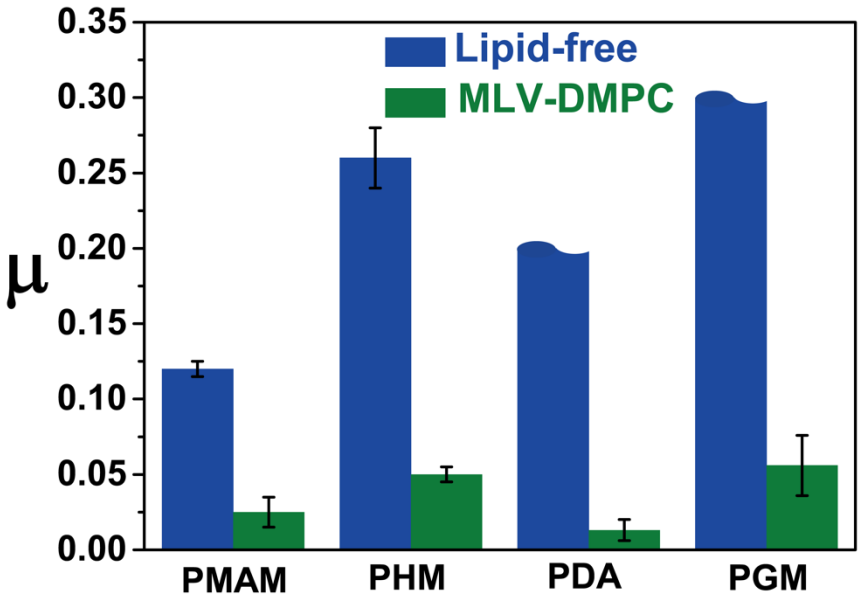

Fig. S1. Sliding friction coefficients between a stainless steel sphere and the different gels described above. Normal loads F_n were (A) PMAM: 5 N. (B) PHM: 0.1 N. (C) PDA: 0.1 N. (D) PGM: 0.1 N.

Fig. S2.

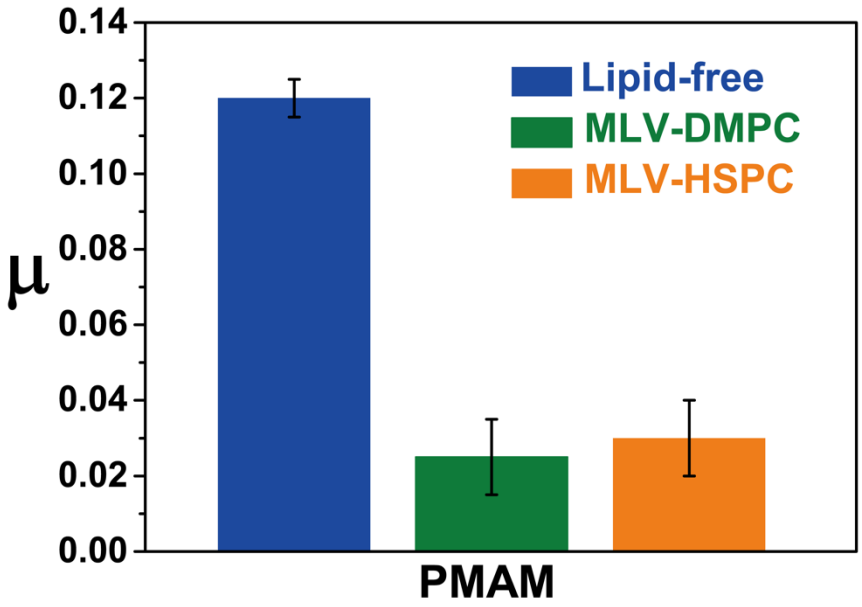

Fig. S2. Sliding friction coefficients between a stainless steel sphere and the PMAM hydrogel, incorporating either DMPC or HSPC lipids (load 5 N).

Fig. S3.

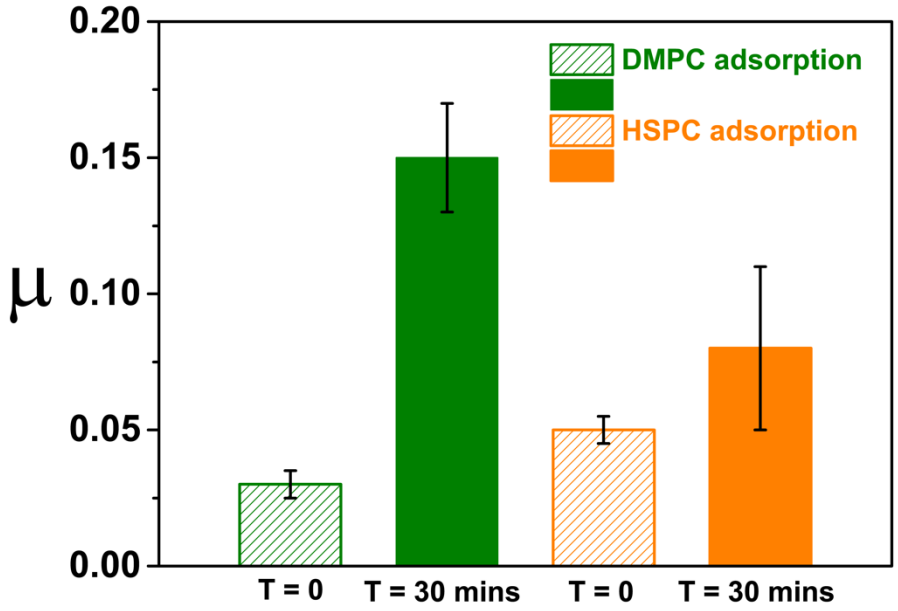

Fig. S3. Sliding friction coefficients between a stainless steel sphere and pHEMA hydrogel, incorporating either DMPC or HSPC lipids, initially (after overnight incubation in lipid dispersion and washing, t = 0), and following 30 mins sliding (load 10 N).

Fig. S4(A).

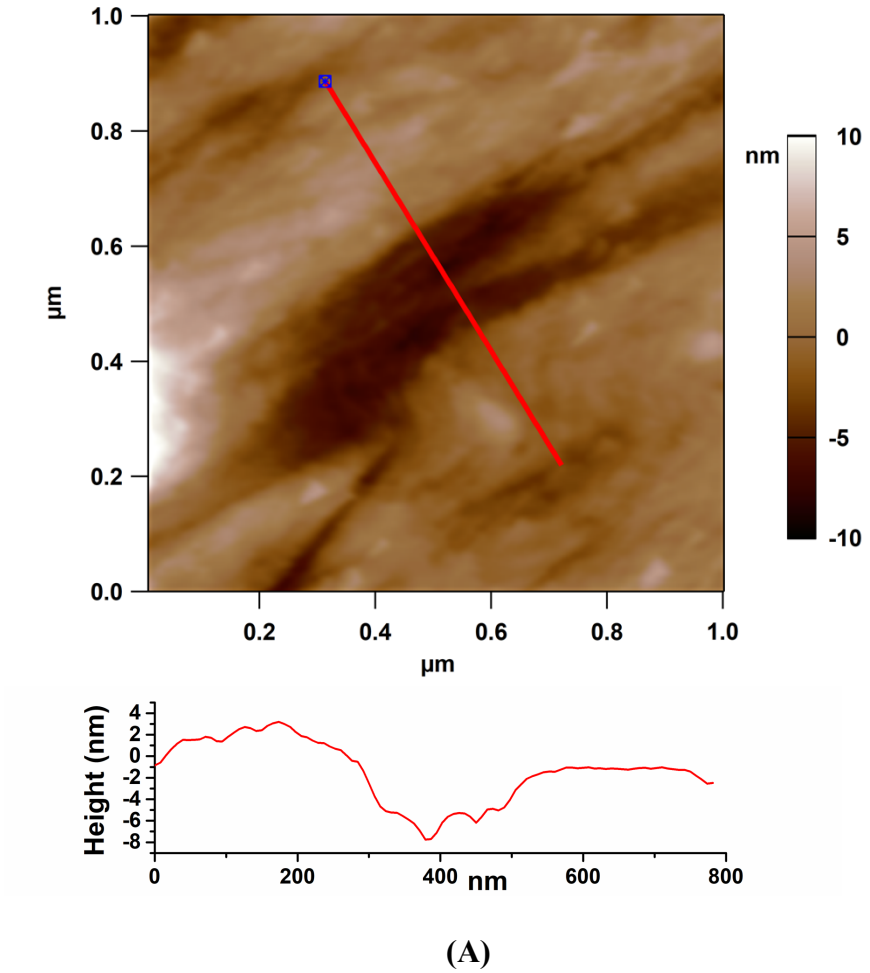

(A)

Fig. S4(A): Tapping-mode AFM image of bare stainless-steel head

Fig. S4(B).

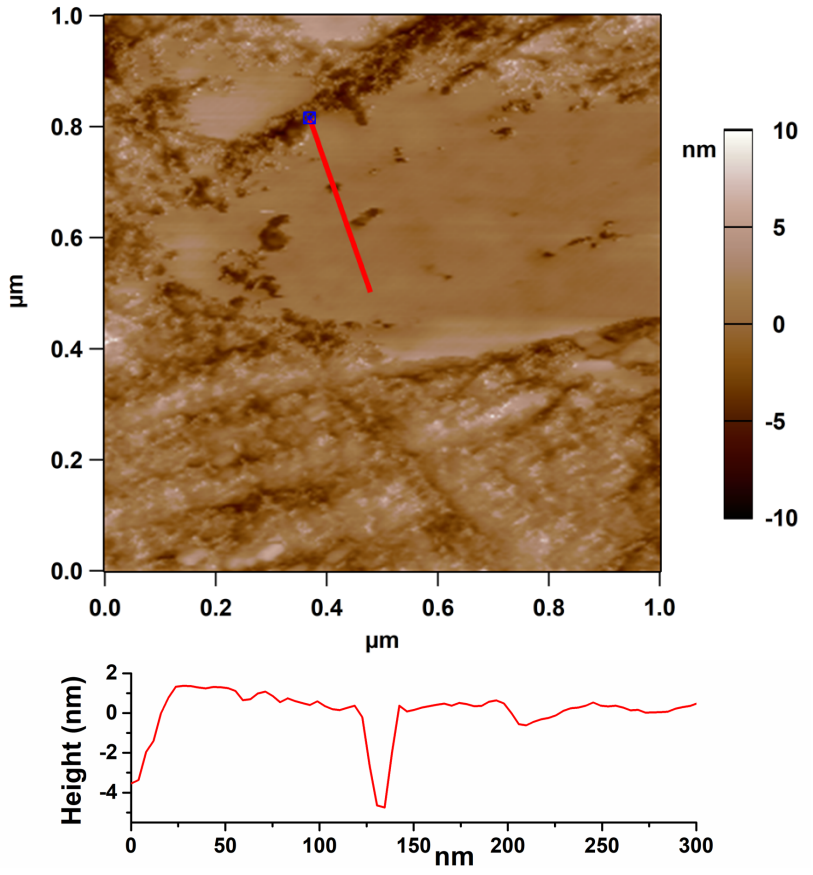

(B)

Fig. S4(B): Tapping-mode AFM image of stainless steel head following 3 hrs incubation in DMPC-MLV dispersion.

Fig. S4(C)

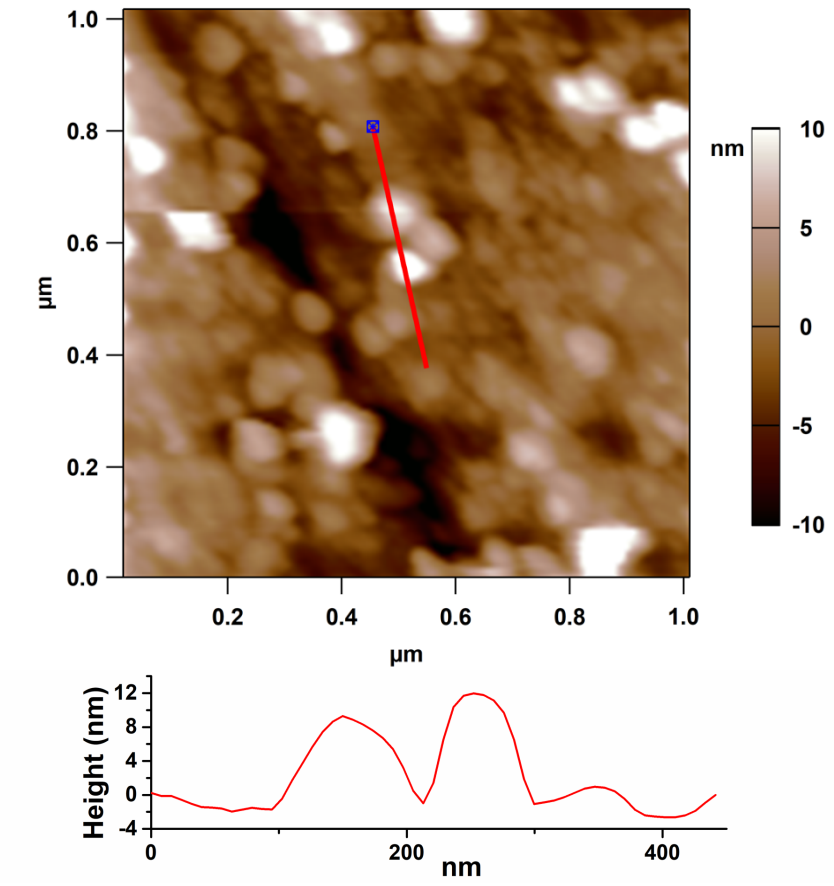

(C)

Fig. S4(C): Tapping-mode AFM image of stainless steel head following 3 hrs incubation in HSPC-MLV dispersion.

Fig. S5.

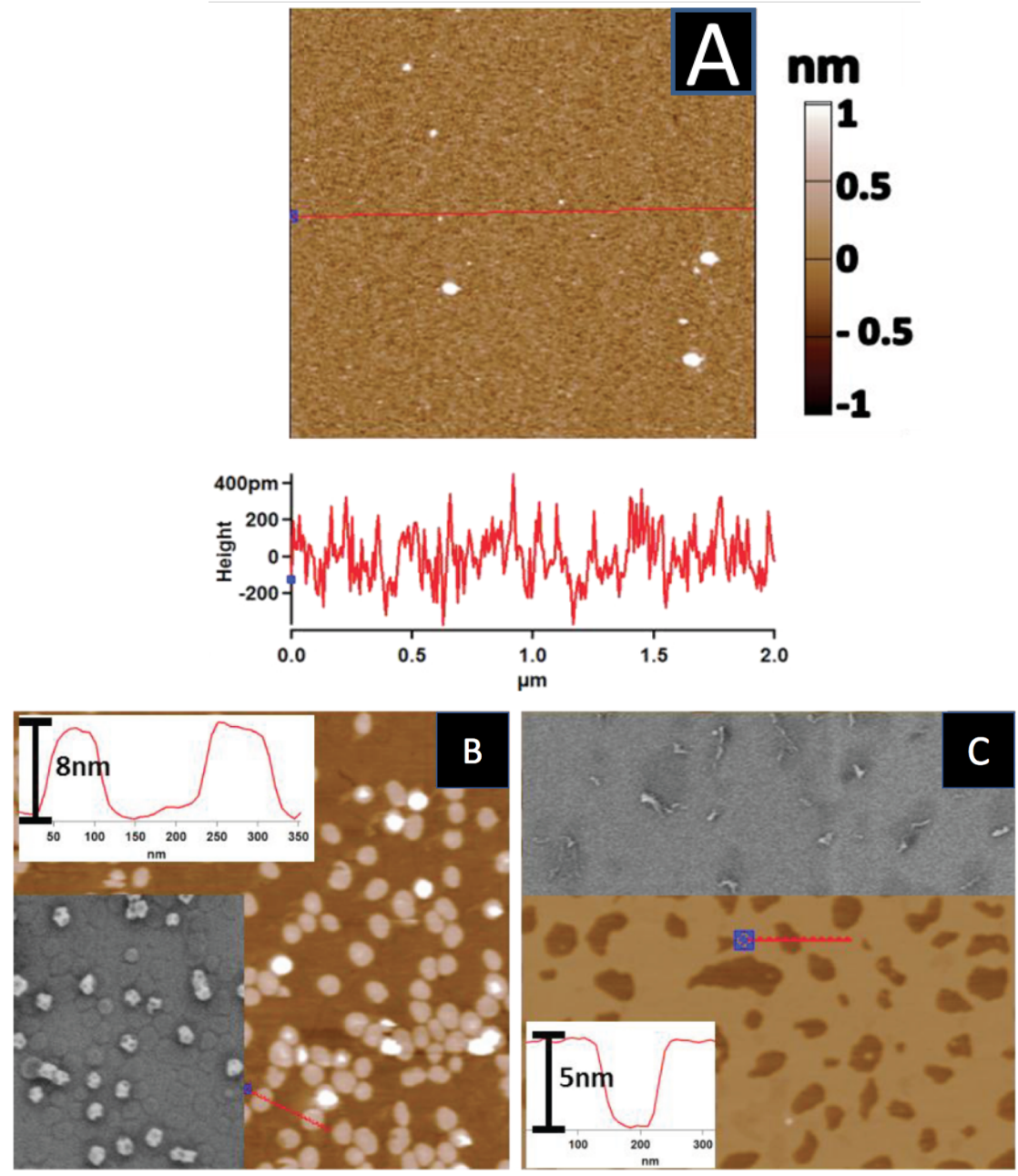
A
nm
1
0.5
0
- 0.5
-1
400pm
200
0
-200
Height
0.0
0.5
1.0
1.5
2.0
µm
B
8nm
50
100
150
200
250
300
350
nm
C
5nm
100
200
300
nm

Fig. S5. AFM micrographs of: (A) pHEMA coated mica surface following overnight incubation in pHEMA solution. (B) pHEMA-coated surface as in (A) following overnight adsorption in HSPC–SUV dispersion followed by washing. Inset lower left is the cryo-SEM micrograph of the same surface. (C) pHEMA-coated surface as in (A) following overnight adsorption in DMPC–SUV dispersion followed by washing. Inset top is the cryo-SEM micrograph of the same surface.

Fig. S6.

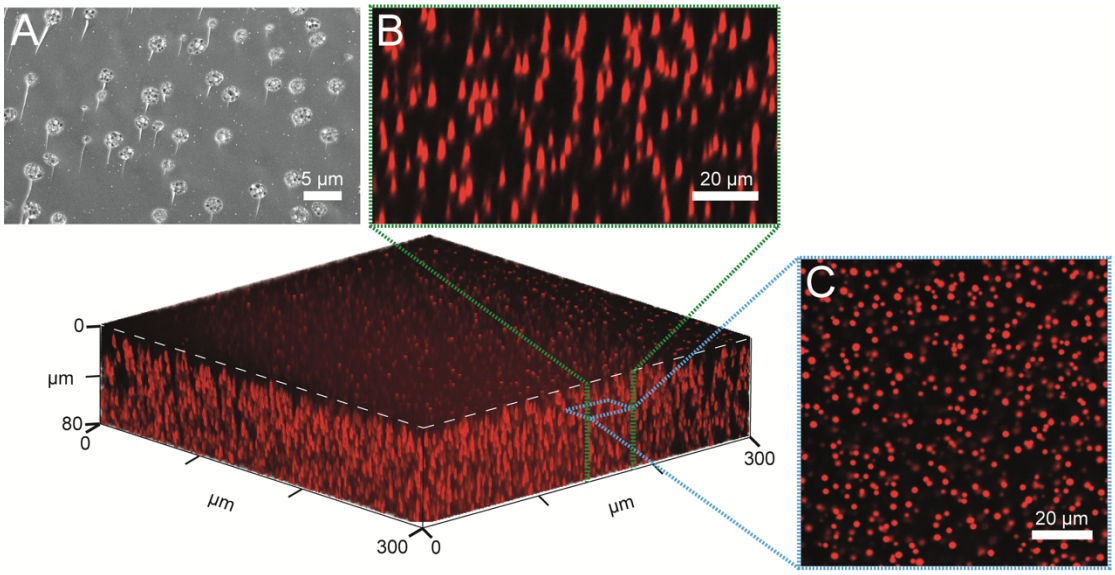

Fig. S6. Confocal microscopy image (Methods, section 6) showing sections through an 80 µm thick slice of MLV-DMPC incorporating pHEMA gel. (A) shows for comparison a section similar to (B) but taken with freeze-fracture cryo-SEM (Methods section 5 and main text figure 2B). (C) is a section parallel to the slice (main text fig. 2D).

Fig. S7.

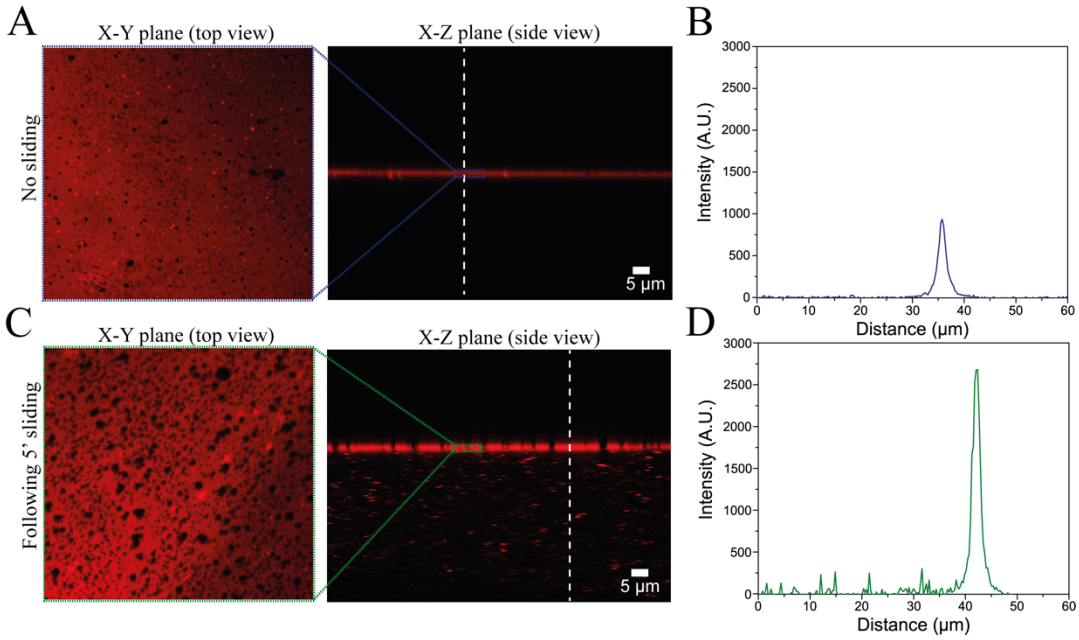

Fig. S7. (A) and (C) show the normalized fluorescence intensity (with background subtracted) on the surface of pHEMA gels incorporating DMPC lipids in micro-reservoirs (top view and side view), for un-rubbed gel surface and for a gel surface over which a stainless steel sphere had been slid, respectively, following 20 mins incubation in a DiI solution. (B) and (D) show the fluorescence intensity scanned through the interface as indicated by the broken white lines in (A) and (C).

Fig. S8.

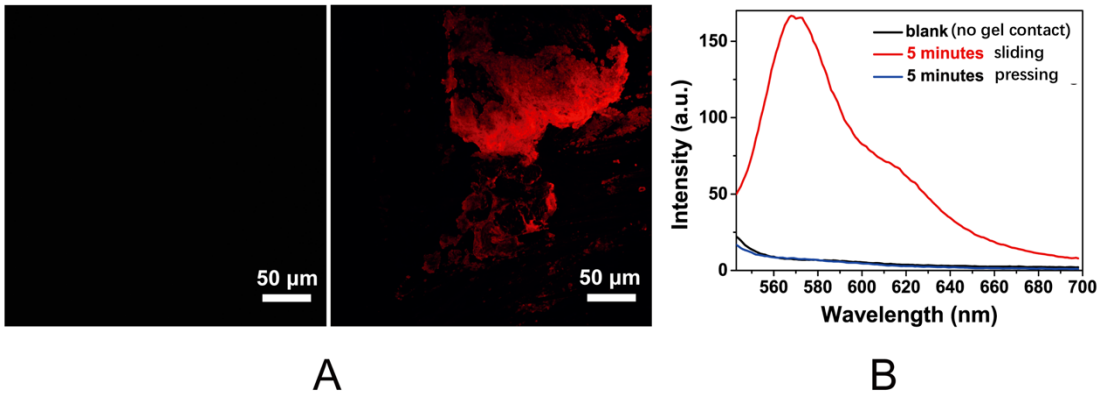

Fig. S8. (A) Confocal microscopy imaging of DiI-labelled lipids transferred to the steel sphere surface after 5 min pressing (left), and after 5 min sliding on DMPC(DiI)-incorporating pHEMA gels. (B) Spectroscopy of the transferred lipids, comparing those transferred to the steel sphere after 5' sliding compared with 5' pressing (no sliding) and with a blank (sphere not in contact with the gel at all).

Fig. S9.

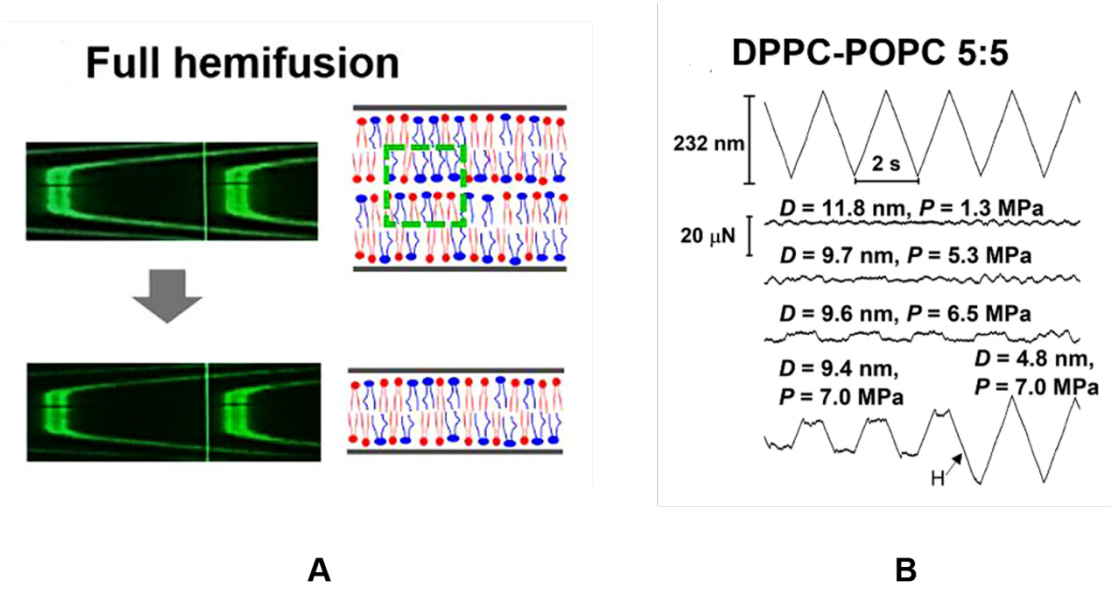

Fig. S9. (A) Schematically showing hemi-fusion between two mica-attached PC bilayers, revealed by the change in surface separation D from 9.4 nm to 4.8 nm as measured from the shift of the interference fringes (left) in the surface force balance (SFB). (B) Simultaneous measurement of the friction between the surfaces seen in the lower friction traces in response to a back-and-forth movement of the upper surface in the SFB. The lowest trace reveals the abrupt increase in friction at the point H corresponding to hemi-fusion as D decreases from 9.4 nm to 4.8 nm (as in A). Adapted from reference (32).

Fig. S10.

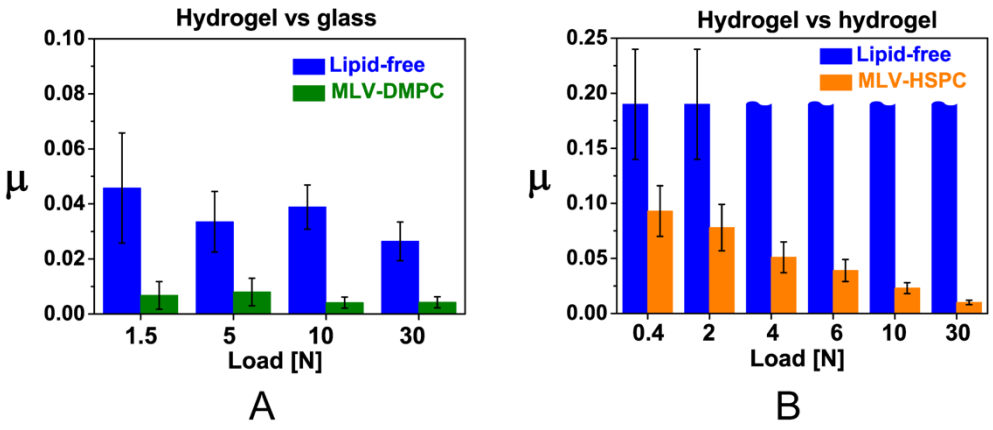

Fig. S10. Showing friction reduction when using counter-faces of different materials sliding against lipid-incorporating pHEMA hydrogel. (A) a 22 mm diameter glass sphere. (B) A symmetric system with pHEMA gels incorporating HSPC-MLVs sliding against a similar lipid-incorporating pHEMA gel.

Fig. S11.

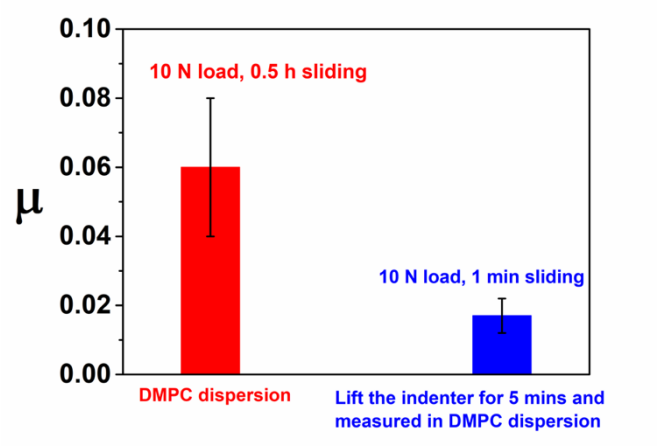

Fig. S11. The higher friction between a spherical steel indenter and a lipid-free pHEMA gel immersed in DMPC-MLV dispersion following 30 mins sliding (left) is strongly reduced (right) once the surfaces are separated for 5 mins and reloaded, as over this period (5 mins) liposomes can again access the depleted contact region.

Fig. S12.

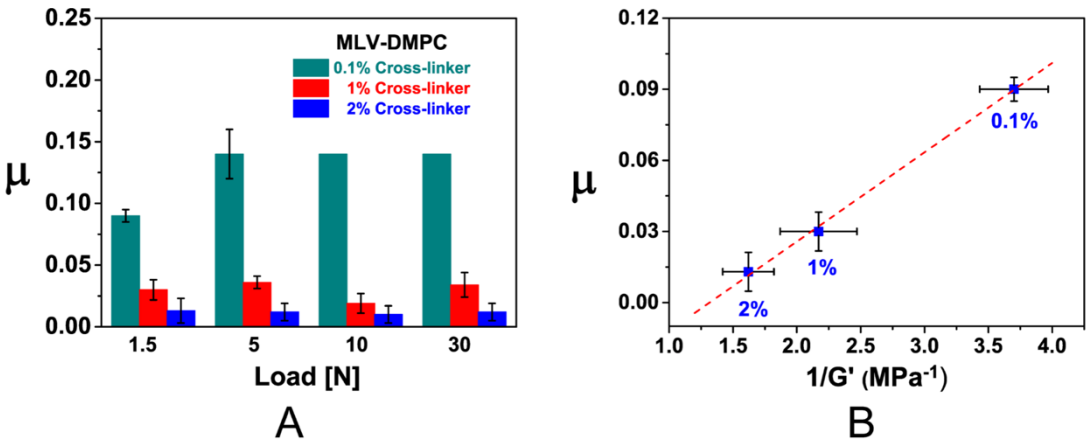

Fig. S12. Variation of the coefficient of friction and shear modulus with cross-linker density. (A) Variation of the coefficient of friction μ with cross-linker density at different loads between a pHEMA gel incorporating DMPC-MLVs and a sliding steel sphere. (B) Variation of μ with inverse shear modulus G' (i.e. with shear compliance) of the gels at 1.5 N load, at different cross-linker%, showing the friction is higher for the softer gels (higher shear compliance; broken red line is guide to the eye).

Fig. S13.

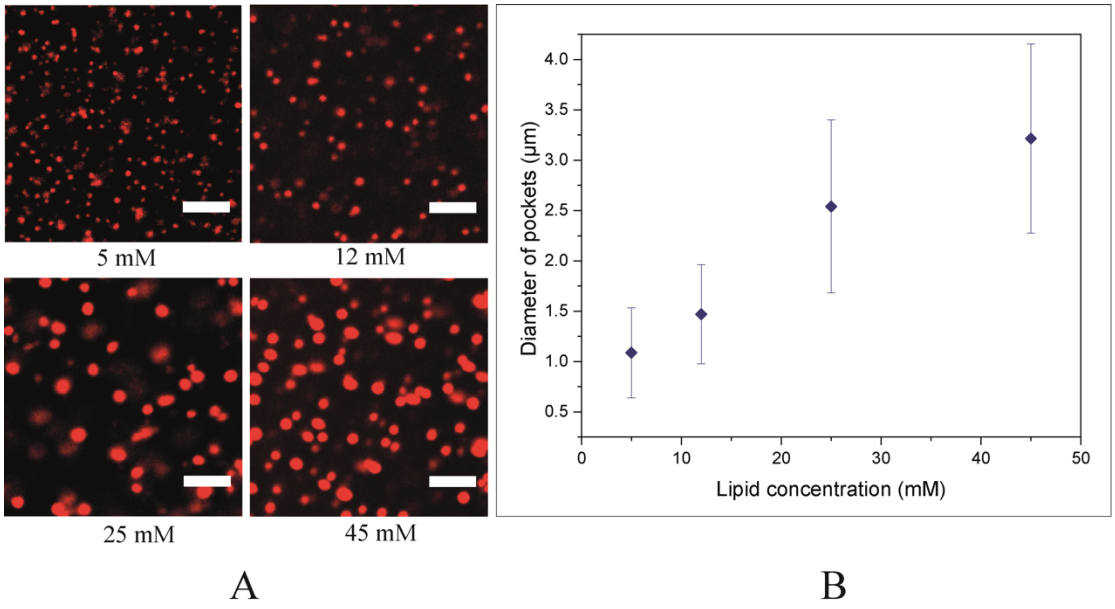

Fig. S13. Showing the effect of concentration of lipids incorporated in pHEMA gels (2% cross-linker) on diameter of the micro-reservoirs. (A) Confocal microscopy of pHEMA gels incorporating DiI-labelled DMPC-MLVs at different concentrations; scale bars 10 µm. (B) Mean diameter of micro-reservoirs as measured from the confocal microscopy; the error bars are standard deviation from the mean.

Fig. S14.

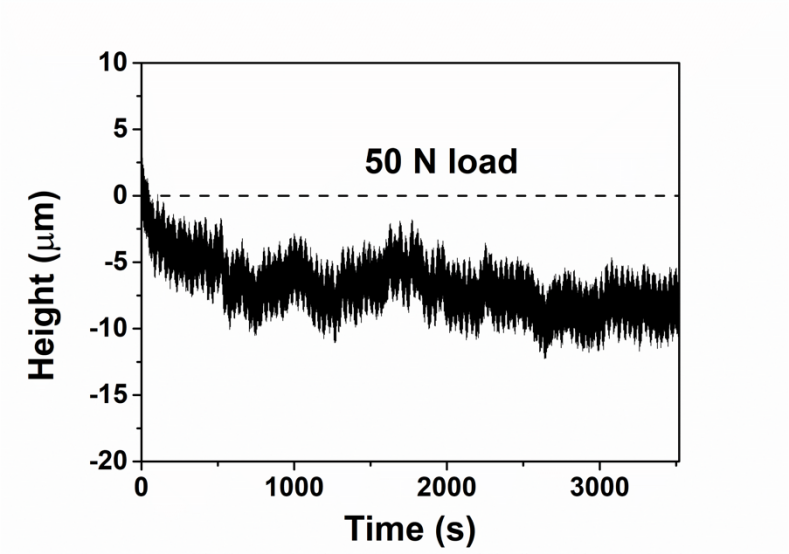

Fig. S14. Wear trace for 50 N-loaded steel sphere sliding on DMPC-MLV-incorporating pHEMA gel for 1 hour (see fig. 4D in main text of ms.). The y-axis indicates the relative height of the stainless steel surface with respect to the gel surface, as monitored directly by the tribometer air-gap capacitor-based sensor (Methods section 7), and its decrease with sliding time corresponds to the wear of the gel.

Fig. S15.

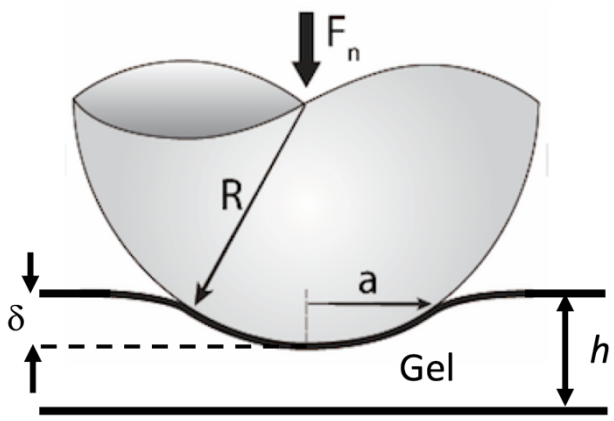

Fig. S15. Schematic of spherical indentation (radius *R*) of gel whose thickness *h* is comparable with or smaller than the contact radius *a*.

Fig. S16.

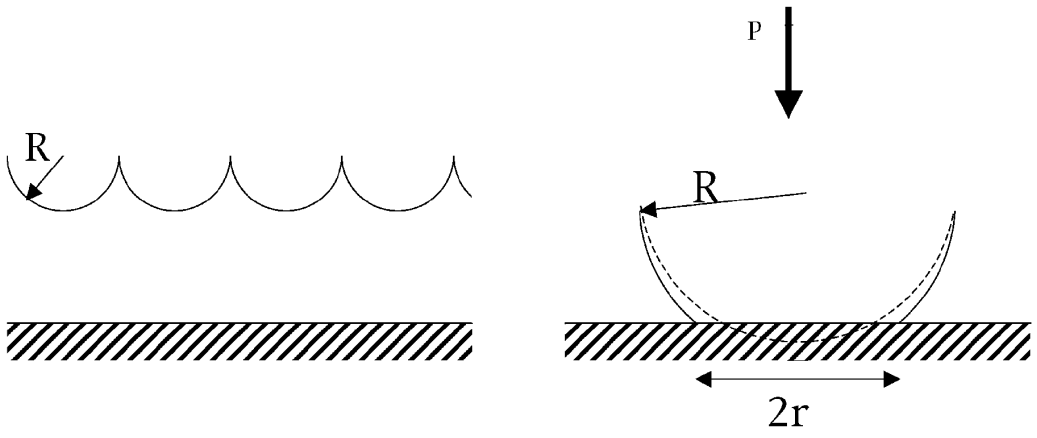

Fig. S16. The left-hand side shows the schematic representation of a rough gel surface (top), compressing against a countersurface, where the roughness is approximated as R. The right-hand side shows a single asperity compressed by pressure P to a flattened contact area of radius r (the broken line denotes the undistorted profile of the asperity).